Clergue, C., Dellinger, M., Buss, H. L., Gaillardet, J., Benedetti, M. F., & Dessert, C. (2015). Influence of atmospheric deposits and secondary minerals on Li isotopes budget in a highly weathered catchment, Guadeloupe (Lesser Antilles). Chemical Geology, 414, 28-41. [17673]. DOI: 10.1016/j.chemgeo.2015.08.015

Influence of atmospheric deposits and secondary minerals on Li isotopes budget in a highly weathered catchment, Guadeloupe (Lesser Antilles)

C. Clergue[1], M. Dellinger[1†], H. L.Buss[2], J. Gaillardet[1], M. F. Benedetti[1], C. Dessert[1]*

[1]Institut de Physique du Globe de Paris (IPGP), Sorbonne Paris Cité, Université Paris-Diderot, UMR 7154, CNRS, 75205 Paris, France

[2]School of Earth Sciences, University of Bristol, Wills Memorial Building, Bristol BS8 1RJ, UK

† Now at Department of Earth Sciences, University of Southern California, 3651 Trousdale Parkway, Los Angeles, California 90089, USA

* corresponding author: E-mail address: clergue@ipgp.fr (Céline Dessert)

Keywords : Lithium isotopes, critical zone, tropical watershed, Saharan dust, chemical weathering, mass balance

Abstract:

To better constrain Li dynamics in the tropics, we sampled critical zone compartments of a small forested andesitic catchment in Guadeloupe (soils, parent rock, atmospheric dust, plants, soil solutions, stream and rain waters). The aims of this study are to identify the origin of Li in the different compartments and to better characterize the behavior of Li and its isotopes during water-rock interaction in a highly cation-depleted soil. The Li isotope signature (δ^7Li) of throughfall samples varies between +11.2‰ and +26.4‰. As this is lower than the seawater signature (31‰) and vegetation does not fractionate Li isotopes, our data indicate that Saharan dust (-0.7‰) significantly contributes to the throughfall signature.

Li isotope composition measured in a 12.5 m deep soil profile varies from +3.9‰ near the surface to -13.5‰ at 11 m depth. Compared to unweathered andesite (+5‰), the deep soil signature is in agreement with preferential incorporation of light Li into secondary minerals. In the top soil however, our results also emphasized that atmospheric deposition (wet and dry)

is a main source of Li to the soil. The decreasing δ^7Li with increasing depth is consistent with a vertical gradient of incorporation of heavy atmospheric Li, this input being maximal near the surface. At the catchment scale, throughfall and total atmospheric inputs (sea salts + Saharan dust) provide 12.1 and 23.9 g Li.yr^{-1} respectively to the Quiock Creek catchment. These fluxes represent 34% and 67%, respectively, of Li exported at the outlet indicating that atmospheric deposition is one of the main Li inputs to the critical zone. Li concentration and isotopic mass balance at the catchment scale indicate that in addition to atmospheric deposition, secondary mineral phase dissolution is a major solute source and that andesite no longer participates in significant production of Li.

Introduction

The evolution of Earth's carbon cycle, climate and habitability is modulated by the concentration of greenhouse gases in the atmosphere, in particular carbon dioxide (CO_2). Over long time scales (10^6 years), neutralization of atmospheric CO_2 by silicate weathering partly controls the variation of atmospheric CO_2 content and thus helps regulate global climate (Walker et al., 1981; Berner et al., 1995). The importance of chemical weathering in controlling the long term evolution of the Earth's climate has stimulated the development of proxies to constrain the weathering history of the continents.

Lithium (Li) and its isotopes have been shown to be sensitive to weathering intensity (Huh et al., 2001; Pogge von Strandmann et al., 2010; Dellinger et al., 2015, Wang et al., 2015) and thus Li seems to be a promising silicate weathering proxy. First, Li is mainly sourced from chemical weathering of silicate rocks in surface waters (Kisakurek et al., 2005; Millot et al., 2010a). In addition, Li is poorly involved in biological processes as it is not a nutrient element. Therefore, its concentration in vegetation is very low and Li isotopes are not fractionated by vegetation uptake (Lemarchand et al., 2010). Moreover, during chemical weathering, Li isotopes are partitioned between secondary mineral and water compartments. The difference between the seawater Li isotopic signature, about 30.8 ± 0.4 ‰ (compilation by Rosner et al., 2007) and the upper continental crust value of 0 ± 2 (1σ) ‰ (Teng et al., 2004) reflects this partition. In general, the dissolved load in both rivers and soil solutions is enriched in ^7Li compared to corresponding river sediments and bedrock, confirming the fractionation of Li isotopes during silicate weathering reactions (Huh et al., 2001, 1998; Tomascak et al., 2003; Kisakurek et al., 2005; Pogge von Strandmann 2010; Wimpenny et al., 2010a; Rad et al., 2013; Dellinger et al., 2015).

In this context, one of the key issues concerning the use of Li isotopes as weathering proxy is to understand the Cenozoic increase of seawater δ^7Li (Misra and Froelich, 2012). Some authors argue that this variation results of modification of δ^7Li of rivers as a consequence of

an increase of global denudation and weathering rates (Misra and Froelich, 2012; West et al., 2014; Pogge von Strandmann and Henderson, 2015). On the contrary, Vigier and Godderis (2015) argue for a stable δ^7Li during the Cenozoic but large change of the Li flux to the ocean during the Cenozoic.

Experimental studies pointed out that while no fractionation is observed during parent rock dissolution (Pistiner and Henderson, 2003; Wimpenny et al., 2010b), the isotopic contrast observed between solution and secondary mineral is due to the preferential incorporation of ^{6}Li in secondary minerals whereas ^{7}Li remains in the residual solution (Pistiner and Henderson, 2003; Wimpenny et al., 2010b; Vigier et al., 2008). It is yet unclear whether this fractionation depends on the nature of the secondary mineral involved (Millot and Girard, 2007; Pistiner and Henderson, 2003, Vigier et al., 2008) or is independent of the mineralogy (Li and West, 2014; Dellinger et al., 2014). Another parameter susceptible to influence the intensity of Li isotopic fractionation is the residence time of water in the subsurface environment (Liu et al., 2015).

Despite the abundance of riverine Li originating from weathering, atmospheric input can significantly contribute to the surface water Li budget (Lemarchand et al., 2010; Witherow et al., 2010). For instance, in the Strengbach catchment (Vosges Mountains, France), 25% of the Li exported at the outlet has an atmospheric origin. At the soil scale, two distinct behaviors of Li isotopes have been proposed. In soils with a high abundance of evolved secondary minerals (with high Al/Si ratio), the soil Li isotope signatures (δ^7Li) are usually low values relative to the unweathered parent rock (Rudnick et al., 2004; Kisakurek et al., 2004; Huh et al., 2004; Liu et al., 2013). In contrast, the Li isotope composition of immature soils (i.e. rich in primary minerals) is not fractionated relative to bedrock samples (Huh et al., 2004; Lemarchand et al., 2010; Pogge von Strandmann et al., 2012). However, the interpretation of soil profiles is made difficult by the uncertainty about the contribution of atmospheric deposits, including marine aerosols (Pistiner and Henderson, 2003; Huh et al., 2004; Teng et al., 2010; Pogge von Strandmann et al., 2012) and atmospheric mineral dusts (Kisakurek et

87 al., 2004; Liu et al., 2013; Huh et al., 2004), both can shift the isotopic signature of the bulk
88 soil. Despite the fact that atmospheric inputs can significantly contribute to soil solutes (e.g.,
89 Widory et al., 2005; Millot et al., 2007), very little atmospheric data exists for non-traditional
90 stable isotope systems as pointed out by Millot et al. (2010b).

91 In order to better characterize Li atmospheric inputs and to investigate their influence on Li
92 isotopes as a weathering proxy, we analyzed here the Li isotopic fractionation in the Quiock
93 Creek catchment, a tributary of the already well-constrained Bras-David River basin
94 (monitored within the framework of the French Critical Zone Observatory) on the Caribbean
95 island of Guadeloupe. This study contributes to a coordinated effort to better constrain new
96 weathering isotopic proxies (Opfergelt et al., 2012; Dessert et al., 2015) and to quantify
97 weathering rates in Guadeloupe at different scales (Rad et al., 2006; Sak et al., 2010; Lloret
98 et al., 2011; Gaillardet et al., 2011; Ma et al., 2012; Dessert et al., 2015). In this study, we
99 measured Li fluxes and isotopic signatures of all the dissolved and solid compartments of the
100 small andesitic watershed of Quiock Creek. As is common for Caribbean islands, this
101 catchment is characterized by a high weathering intensity and relatively important
102 atmospheric inputs of both dust of Sahara origin and sea salts. In this context, we show that
103 atmospheric inputs of Li provide up to 67% of the Li exported at the outlet and that secondary
104 mineral weathering also contributes to the Li budget. We provide the first measurements of
105 δ^7Li for Saharan dust deposited in Guadeloupe. These values are crucial for the
106 determination of the global budget of Li in areas that are severely impacted by Saharan
107 dusts, such as the Caribbean region and Amazon basin.

108 1. Site description

109 The Quiock Creek catchment (16°17'N, 61°70'W) is lo cated on Basse Terre Island, the
110 volcanic part of the Guadeloupe archipelago in the French West Indies (Figure 1). The study
111 site (area of 8ha) is located in the primary tropical rainforest of the Guadeloupe National Park
112 at an elevation ranging from 200 m to 350 m. Quiock Creek is a small tributary of the Bras-

David River monitored by the ObsErA observatory (INSU-CNRS CZO) dedicated to the study of weathering and erosion processes under tropical climatic conditions (Lloret et al., 2011; 2013; Dessert et al., 2015).

The Quiock Creek catchment has a wet tropical climate with two seasons: the dry season, from January to June, and the cyclonic wet season, from July to December. The mean annual temperature and precipitation rate measured on site for the last 2 years are 25 ℃ and 3500 mm yr^{-1} respectively. The annual runoff ranges from 700 mm to 2800 mm with a mean annual value of 1130 mm. Evapotranspiration is high, around 63 %, which is typical for a tropical rainforest (Roche, 1982; Loescher et al., 2005, Lloret et al., 2011) and is likely due to the high frequency of low intensity short duration rainfalls and convective transport of evaporated moisture as shown to be the case in similar Caribbean tropical forests (Schellekens et al., 2000). Tropical storms and hurricanes also contribute significantly to the hydrology of the site (Zahibo et al., 2007). For instance, during hurricane Rafael (13-14 October 2012), 141 mm of rainfall in 48 h were measured on site, corresponding to 5% of the total annual rainfall.

The Quiock Creek catchment lies on Pleistocene andesitic pyroclastic deposits (Boudon et al., 1988) that are covered by a very thick ferralitic soil (>15 m thick; Colmet-Daage and Bernard, 1979, IRD soil map; Buss et al., 2010). Although these deposits are not dated, the age of adjacent volcanic flows is 1.46 Myr before present (Samper et al., 2007). The soil profile of Quiock Creek consists of highly weathered volcaniclastic debris flows containing andesitic clasts at various stages of weathering (Buss et al., 2010; Sak et al., 2010; Ma et al., 2012). A previous study showed that secondary minerals are dominant and represent 95 wt.% of the bulk soil (Buss et al., 2010). Clays corresponding to kaolinite and dominantly halloysite, account for 70 wt.% of the mineralogy and non-clay secondary minerals are almost entirely Fe(III)-hydroxides (approx.. 19 wt.%) and gibbsite (concentration is highly variable along the profile). Primary minerals consist of quartz (0-8 wt.%), feldspar (0-4 wt.%) and cristobalite (mean of 3 wt.%) (Buss et al., 2010). Quartz and feldspars (dominantly

orthoclase) are primarily found in the upper 30 cm of the profile and, concomitantly, in several deeper levels but quartz content is otherwise very low and feldspar largely absent in the rest of the profile. The soil is highly depleted in soluble cations (Buss et al., 2010), but despite the high nutrient depletion of these soils, the tropical rainforest vegetation is dense and the mean litter flux is high (7.8 t ha^{-1} yr^{-1}, Rousteau, 2014) comparable to a similar rainforest in northeastern Puerto Rico (Weaver and Murphy, 1990).

One of the peculiarities of the Quiock Creek catchment is the input of both Saharan dust and volcanic ash. Montserrat volcano, located 86 km NW of Guadeloupe, erupted on July 18th 1995, after a century of quiescence and is still currently active. Since 1995, six ash fall episodes were recognized that had consequences in Guadeloupe (www.mvo.ms; activity report OVSG 2000). The two most important events took place in September 1996 and February 2010 and produced ash-fall deposits over Guadeloupe Island that were thicker than 1mm, corresponding to fluxes of about 100 g m^{-2} of ash each (OVSG and personal communication of J.C. Komorowski). The other exogenous input to the top soil comes from the Sahara desert. This flux, measured in Guadeloupe, is around 100 kg ha^{-1} yr^{-1} (J. Molinié, personal communication) and is consistent with literature values varying between 50 and 200 kg ha^{-1} yr^{-1} in the Caribbean basin (Glaccum and Prospero, 1980; Mahowald et al., 2006; Pett-Ridge et al., 2009). The Saharan dust deposits are mainly composed of mica/illite and quartz with lesser amounts of kaolinite, chlorite, montmorillonite, microcline, plagioclase, and calcite (Prospero et al., 1970; Glaccum and Prospero, 1980). These deposits contribute significantly to the formation of many soils in the Caribbean and Amazon Basin (Borg and Banner, 1996; Herwitz et al., 1996; Muhs et al., 2009; Pett-Ridge et al., 2009). In Guadeloupe, the dull aspect of quartz in the soil, characteristic of aerial transport, suggests that Saharan dust is likely the source of quartz to the soil profile, although chemical weathering of quartz can also alter grain surfaces and is known to occur in thick tropical soils (e.g. Schulz and White, 1999).

2. Sample collection

167 This study is based on the quantification and geochemical characterization of water fluxes
168 entering, passing through and leaving the catchment. The precipitation rate above the
169 canopy (openfall) was measured on site with a rain gauge in a clearing in the vicinity of the
170 sampling site. The rain gauge measured events of minimum 0.2 mm of rainfall per hourly
171 step. The throughfall flux was measured every two weeks for two years (06-2011 to 08-
172 2013), using 22 collectors randomly positioned across the site. In this study, 131 water
173 samples were collected: 13 rainfall samples, collected on site (RF-MF) or at the OVSG (RF-
174 OVSG, 15 km southeast of the studied site), 51 throughfall and stemflow samples, 57
175 samples of Quiock Creek stream water and 35 soil solution samples. These samples were
176 collected during contrasting hydrological periods. Throughfall, stemflow and rainwaters were
177 sampled during six field trips between 2011 and 2013. Throughfall and rainwaters were
178 collected in polypropylene bottles with a funnel located one meter above the ground in order
179 to avoid contamination from soil particles. Three throughfall collectors were randomly
180 positioned at the study site. Stemflow samples were collected from silicone gutters set
181 around the trunks of two different trees. However, the sampling device caused Cl
182 contamination thus the stemflow Cl concentration were not taken into account. Quiock Creek
183 samples were collected manually once a month and more frequently during field trips. Soil
184 solutions were sampled once a month from nested tension lysimeters (positioned between
185 15 and 823 cm depth) equipped with porous ceramic cups (see Buss et al., 2010).

186 For all water samples, pH and conductivity were measured on site or at the OVSG. After
187 collection, non-filtered 20 mL aliquots were used for alkalinity measurements. The remaining
188 water samples were filtered through 0.2 µm cellulose filters and divided in two aliquots stored
189 in polypropylene bottles: one non-acidified for anion and silica determination and one
190 acidified to 2% HNO_3 for cation and trace element analyses. Samples for Li isotope
191 measurements were stored in polypropylene bottles previously washed with distilled 0.5N
192 HNO_3 and acidified to 2% HNO_3. Lithium isotopic compositions were measured on 19
193 selected water samples corresponding to 7 samples of throughfall and stemflow, 4 samples

194 of Quiock Creek stream water and 8 samples of soil solution corresponding to two sampling
195 dates (October 26, 2012, and June 28, 2013).

196 Soil samples (n=23) down to 12.5 m depth were collected with a hand-auger during lysimeter
197 installation in 2007 (Buss et al., 2010). As the auger did not encounter fresh andesite at the
198 bottom of the profile; we analyzed andesite from Samper et al. (2007) (sample 04-GW-12) to
199 characterize the unweathered parent rock. Ash from Montserrat volcano was collected at the
200 OVSG during the February 2010 eruption. During a Saharan dust event in July 2013, we
201 collected rainfall particulate matter by filtration on a 0.2 µm cellulose filter, which was then
202 dried and stored in a Petri dish. Finally, 7 vegetation samples were analyzed (litter, branches
203 and roots). Litter samples chosen for analysis correspond to the most productive period
204 between the 10^{th} and the 24^{th} of June 2011. Lithium isotopic compositions were measured in
205 all of these solid samples but only in 13 soil samples. Finally, Nd isotopic compositions were
206 measured in 6 samples of the soil profile.

207 3. Analytical methods

208 3.1 Sample preparation for analyses

209 3.1.1 Solid sample digestion

210 Soil and vegetation samples were first dried in an oven (60°C) for 3 days and crushed in an
211 agate mortar (soil samples) or in a ball mill (vegetation samples). For soils, volcanic ash and
212 rocks, 100 mg of each sample was dissolved in a mixture of HNO_3/HF for 2 days at 120 °C.
213 This mixture was then evaporated and dissolved twice in 2mL 6N HCl and finally stored in 1N
214 HCl. Saharan dust samples collected on cellulose filters were treated with the same protocol
215 but with an initial step of filter digestion in diluted 5N HNO_3 at 100°C for 1 day. Vegetation
216 samples (about 0.5 g) were dissolved in 10 mL of HNO_3 in 50 mL Teflon beakers and
217 digested in a DigiPREP block digestion system for 24h at room temperature and another 24h
218 at 90°C. These samples were then evaporated at 60°C and dissolved once more in 16N

219 HNO_3 for 24h at 90°C. Finally, after evaporation, 0.5 m L HF/ H_3BO_3 were added to fully
220 dissolve phytoliths. These samples were then stored in 50 mL of 2N HNO_3.

221 3.1.2 Li and Nd purification

222 For Li isotopes, the evaporated volumes were calculated to reach 20 ng of Li in 1 mL. Water
223 samples were first evaporated to dryness and digested in HNO_3 to remove the organic
224 matter. Then the protocol is the same for water and solid samples. Lithium was separated
225 from the rest of the matrix by ion-exchange chromatography with a Biorad AG50X-12 resin
226 and a 0.2N HCl eluent following the protocol detailed in Dellinger et al. (2014) (modified from
227 James and Palmer, 2000).

228 The separation of Nd from the rest of the matrix is a two-step procedure (Richard et al.,
229 1976; Caro et al., 2006). The first step consists of separation of rare earth elements from the
230 rest of the matrix on TRU-Spec resin in 2N HNO_3 media. The second step consists of
231 separation on Ln-spec resin of the different rare earth elements in 0.25N HCl media. The
232 purified solution of Nd is then evaporated and dissolved in 3N HNO_3 for isotopic
233 measurement. The minimum quantity of Nd in purified solution is 50ng in 1 mL (50ppb).

234 3.2 Major and trace elements analyses

235 Base cations were measured by ICP AES (Thermofisher iCap 6200 series) at the Institut de
236 Physique du Globe de Paris (IPGP). Anions in soil solutions were measured with a Dionex
237 DX 120 chromatograph at the IPGP and the OVSG/IPGP. Dissolved Li concentrations were
238 measured using HR-ICP-MS (Element II ThermoScientific) at IPGP. The limit of
239 quantification is estimated to be 20 ppt and the accuracy was controlled by repeated
240 measurement of the SLRS-5 standard with an external reproducibility of 3%. Trace elements
241 in solid samples were measured with an ICP-MS X series mass spectrometer (Thermo
242 Electron) at the Institut des Sciences de la Terre de Paris (ISTeP) of the University of Pierre
243 et Marie Curie (UPMC). We followed the bracketing method using rock standards BEN for
244 bracketing and BEN, GSN, BCR-2, BHVO2 and JB-2 to validate the measurements. The

standard values measured in this study are compared to the certified values to validate the data (Table 1S). Major element and Li concentrations in litter samples were measured by a calibration curve, such as for water samples. The accuracy of this measurement was checked by repeated analyses of a vegetation standard NIST SRM 1515 (apple leaves).

3.3 Li isotope analyses

Li isotope analyses were performed on the Neptune multicollector ICP-MS (Thermo Scientific) at IPGP using the Apex sample inlet system. The δ^7Li is calculated relative to the L-SVEC standard (Flesh et al., 1973) as follows:

$$\delta^7 Li = \left(\frac{\left(\frac{^7Li}{^6Li}\right)sample}{\left(\frac{^7Li}{^6Li}\right)L-SVEC} - 1 \right) \times 1000 \quad (1)$$

Each sample was measured three times and bracketed before and after with the L-SVEC standard, which had the same concentration as the sample (within 10% error).This bracketing sequence yields five δ^7Li values which are averaged to give the δ^7Li of the sample. Three values are obtained using the average L-SVEC values of standard measured before and after the sample. Two supplementary values are obtained using the average value of two sample normalized by the L-SVEC which is measured between the two samples. In addition, IRMM-16 (Qi et al., 1997) and Spec-pure (Dellinger, 2013) Li standards are routinely measured at the beginning and during each sequence. The in-run precision, calculated from repeated measurements, is below 0.2 ‰. Indeed, the IRMM-16 standard isotopic composition we measured was 0.17 ± 0.08 ‰ (2σ, n=50) and 94.42 ± 0.12 ‰ (2σ, n=19) for the Li-SPEC standard. Typically, a solution of 20 ppb produces a signal of 8 V and the background was typically less than 50 mV (0.01 ng corresponding to 0.6% of the 20 ppb signal). The blank measured immediately before and after each sample and standard is subtracted. The method used corresponds to the measurement of 8 ratios of 12 seconds iteration time per sample or standard. The external reproducibility, based on repeated measurements of standards is below 0.5‰. The δ^7Li of the NASS-5 seawater standard was

measured at +30.73 ± 0.35‰ (2σ) (n=9 separations and measurements) in good agreement with data from the literature (Millot et al. 2004; Rosner et al., 2007; Huang et al., 2010). A homemade standard, called SLC, corresponds to L-SVEC mixed into a multi-element matrix in order to reproduce the mean river composition and was measured at -0.11 ± 0.27‰ (2σ) (n=16 separations and measurements). Standard basalt BHVO-2 samples were measured at +4.33 ± 0.43‰ (2σ) (n=6, 6 separations), in good agreement with the data from the literature (Jeffcoate et al., 2004 ; Penniston-Dorland et al., 2012 ; Vlastelic et al., 2009 ; Dellinger, 2013). Finally, the procedural blank is lower than 0.05 ng of Li, negligible compared with the 20 ng of Li from the sample.

3.4 Nd isotope analyses

Nd isotope analyses were performed on the Neptune multicollector ICP-MS (Thermo Scientific) at IPGP using the Apex sample inlet system. The εNd is calculated relative to the CHUR (Chondritic Uniform Reservoir) as follows:

$$\varepsilon_{Nd} = \left(\frac{\frac{^{143}Nd}{^{144}Nd}_{sample}}{\frac{^{143}Nd}{^{144}Nd}_{CHUR}} - 1 \right) \times 10\,000 \quad (2)$$

The CHUR value is 0.512638 (Jacobsen and Wasserburg, 1980). The method used corresponds to the measurement of 100 ratios of 4 seconds iteration time per sample or standard. Mass interferences with Sm (144, 148 and 150) were corrected using $^{147}Sm/^{144}Sm$ = 4.83870. The mass bias was corrected using the $^{146}Nd/^{144}Nd$ ratio of 0.72190. Each measurement was normalized to the NIST value certified as $^{143}Nd/^{144}Nd = 0.511418 \pm 6\ 10^{-6}$ (Caro et al., 2006) which is measured every 3 samples. The external error is 0.18 ε (2σ).

4. Results

4.1 Major and trace element concentrations

4.1.1 Water samples

Major element and Li concentration data are presented in Table 1 for samples for which Li isotopic composition was measured. Concentrations of major elements and Li in all the other samples measured during this study are presented in Table 3S. All samples have low pH ranging from 3.6 for a stemflow sample to 6.3 for a throughfall sample. Stemflow samples have the highest major element concentrations. The later are probably due to organic matter leaching from the tree surface during the water flow. Along this sinuous pathway, strong interactions between water and tree surface take place and can induce water evaporation, contributing thereby also to increase concentrations. Li concentrations vary between 2 and 20 $nmol.L^{-1}$ in rainfall (RF) and throughfall (TF). The median Li concentration in rainfall (5 $nmol.L^{-1}$) is lower than in throughfall (7 $nmol.L^{-1}$). These concentrations are in the low range of the literature data for volcanic island (Louvat et al., 1997; Pistiner and Henderson, 2003; Pogge von Strandmann, 2006, 2010). In comparison, stemflow waters have higher Li contents (29 to 66 $nmol.L^{-1}$). Soil solution (SS) is the dissolved compartment with the highest Li concentrations between 41 and 121 $nmol.L^{-1}$ (mean $[Li]_{SS}$= 77 $nmol.L^{-1}$). Finally Quiock Creek (QC) samples have Li concentrations ranging between 38 and 72 $nmol.L^{-1}$ (with a mean value of $[Li]_{QR}$= 56 $nmol.L^{-1}$). For RF and TF samples, Cl concentrations are well-correlated with Na concentrations (Figure 2, r^2=0.97) and plot close to the dilution line of seawater. This indicates that both Na and Cl in RF and TF originate mostly from sea salt and are not influenced by the vegetation. The molar Li/Cl ratios of RF and TF, ranging from 4 10^{-5} to 13 10^{-5}, are higher than the seawater ratio (Figure 3) and thus show that sea salts are not the only source of Li in the rain. The Li/Cl ratios measured in RF and in TF have similar ranges, but are higher in the soil solutions and the Quiock Creek water samples. Dessert et al. (2015) demonstrated that Cl behaves conservatively in Basse-Terre watersheds, therefore our observation indicates that in addition to rain, another source contributes lithium to soil solutions and to Quiock Creek. Moreover, Li/Cl ratios in soil solution samples are more variable than in Quiock Creek samples. The fact that Quiock Creek integrates solutes

derived from a larger surface area and over a longer time-scale than the soil solution compartment could explain this observation.

4.2.2 Soil, rock and vegetation samples

Table 2 reports major element and trace element concentrations together with Li isotopic composition in Saharan dust, volcanic ash, litter, soil and rock samples. Saharan dust has the highest Li concentration of this sample set with a mean Li content of 18.5 ppm. This value is in agreement with those found in the literature (Moreno et al., 2006; Trapp et al., 2010). The Li concentration in the local andesite is 12 ppm, also in good agreement with the characteristic range for andesite in the literature (Magna et al., 2004; Schuessler et al., 2009; Halama et al., 2009). Montserrat volcanic ash has the same Li concentration as andesite, consistent with the andesitic origin. In vegetation samples, the Li concentration is low and relatively constant in all plant compartments with a mean Li concentration of 0.3 ppm, consistent with values found in the literature (Lemarchand et al., 2010; Vetter et al., 2005). Soil samples have Li contents between 5 and 15 ppm. To correct for dilution effects and volume change, Li concentrations in soil samples are normalized to an immobile element (Ti) and to a mobile element (Na). In Figure 4a and 4b mass transfer coefficient (τ) values are presented for major elements and Li :

$$\tau = [(X/Ti)_{soil} / (X/Ti)_{andesite}] - 1 \quad (3)$$

and represents the depletion of X (element of interest) in the soil compared to the andesite. If τ is <0, X is depleted in the soil relative to the andesite and if τ is >0, X is enriched in the soil relative to the andesite (Brimhall and Dietrich, 1987). Figure 4a shows that Li and other soluble elements are depleted in the soil relative to andesite. However Li is less depleted (τ = -0.6) in the soil than the major elements (τ < -0.85, where τ = -1.0 indicates total depletion). Moreover, Li/Na ratios in the soil profile compared to the ratio in andesite (4c) shows that Li is less depleted than Na. These observations indicate that Li is lost from the bedrock during water rock interaction in agreement with its soluble behavior, but is less mobile than the other

soluble elements reflecting its incorporation into secondary minerals. Additionally, Li and other mobile elements are notably less depleted in the bottom 15 cm of the soil profile and at 305 cm, 427 cm, 1219 cm and 1250 cm depth.

4.2 Nd and Li isotope compositions

Nd isotopes in the soil displayed ε_{Nd} values between -8.39 and 2.71 (Table 2). The very negative values of ε_{Nd} are very different from values characteristic for andesite (Figure 4), implying that an exogenous source contributes to Nd budget in the soil. Indeed, these particular values are close to ε_{Nd} of Saharan dust. Two soil depths exhibit the Saharan dust-like Nd signature: the most superficial at 15 cm depth and the 305 cm depth. These depths correspond to levels enriched in quartz and feldspar, which are also less depleted in mobile elements and Li. The presence of quartz associated with the relatively higher concentrations of mobile elements and the isotopic signature of Nd provide independent lines of evidence for dust layers at discrete depths well below the soil surface. The only way to explain dust mineral inputs below about 1 meter depth is if the soil profile developed from a bedrock profile that comprising multiple episodes of volcanic deposition, with quiet periods of dust deposition in between. Zones of dust within the profile thus represent soil paleo-surfaces.

Li isotope signatures in all compartments studied in the catchment are displayed in Figure 5. Throughfall samples have the highest δ^7Li, ranging between +11.2 and +26.4‰. Li isotopic compositions measured in two distinct throughfall samples from the same date are similar, demonstrating the robustness and significance of δ^7Li values. The δ^7Li values of Montserrat volcanic ash are +4.7‰ close to the value of andesite (Halama et al., 2009; Magna et al., 2006; Schuessler et al., 2009). The measured Saharan dust δ^7Li is -0.7‰ consistent with their crustal origin and mineralogy. This value is slightly lower than the δ^7Li of the mean continental crust, which is 0 ± 2 (1σ) ‰ (Teng et al., 2004; Liu and Rudnick, 2011) probably due to the predominance of secondary minerals in these dust samples (70% of mica/illite, kaolinite, chlorite; Glaccum and Propero, 1980) enriched in the light Li isotope. Vegetation

371 δ^7Li is found to vary between +3.6 and +8.7‰, a range that is higher than the one reported
372 by Lemarchand et al. (2010). Li isotope signatures in the solid soil profile are highly variable
373 and can be separated into two zones (Figure 5). The shallower zone, between the surface
374 and 274 cm depth, with a mean signature of +2.9 ± 0.9‰, exhibits no variation as a function
375 of depth. In the deeper zone, between 274 cm and 1097 cm depth, the Li signature
376 decreases regularly with depth from +0.6 to -13.5‰, reaching one of the lowest δ^7Li values
377 ever reported in the literature for soil samples (Pistiner et al., 2003; Rudnick et al., 2004; Huh
378 et al., 2004; Lemarchand et al., 2010; Pogge von Strandmann et al., 2012; Liu et al., 2013).
379 Li isotope signatures in the solid soil are systematically more negative than in andesites. Soil
380 solution δ^7Li varies between +4.6 and +8.9 ‰ with no trend with depth. The measured δ^7Li of
381 andesite is consistent with values reported for andesite in the literature (Halama et al., 2009;
382 Magna et al., 2006; Schuessler et al., 2009). Quiock Creek water samples have a relatively
383 constant δ^7Li value of +8.2 ± 0.6‰, close to the soil solution value, suggesting that Quiock
384 Creek Li is essentially supplied by the soil solution. The Quiock Creek δ^7Li falls in the low
385 range reported in the literature for rivers draining volcanic rock (Rad et al., 2013; Henchiri et
386 al., 2014).

387 4.3 Water budget

388 The mean annual rainfall is 3500 mm yr^{-1} (ObsErA database). The yearly average throughfall
389 flux varies significantly between the two years studied: 3530 mm yr^{-1} for the first year (June
390 2011 to June 2012) and 2990 mm yr^{-1} for the second year (June 2012 to June 2013). We
391 used a sliding average to estimate a mean throughfall flux of 3079 ± 660 mm yr^{-1}.

392 Unlike throughfall, stemflow flux cannot be accurately estimated because of the difficulty in
393 determining the water interception surface of the trees. The discharge of the catchment was
394 measured ten times in the Quiock Creek and was found to vary between 150 and 400 $L.min^{-1}$
395 . In order to determine a more precise discharge, Cl is used as a conservative element
396 (Dessert et al., 2015). We considered that the flux of Cl that enters the catchment is leaving it

397 without significant loss. As we know the throughfall flux, the median throughfall Cl
398 concentration (100 µmol L^{-1}) and the mean Cl concentration in RQ (272 µmol L^{-1}), we can
399 infer the discharge. The calculated discharge is 1130 mm yr^{-1}, corresponding to a flow of 172
400 L min^{-1}, which is consistent with the values episodically measured in the catchment.

401 ## 5. Discussion

402 We have shown that the various compartments in the Quiock Creek catchment have distinct
403 Li concentrations and isotopic signatures. Here, we first discuss and quantify the influence of
404 atmospheric inputs to the Li budget in the catchment. Then we examine their importance at
405 both the profile and catchment scales. Finally, we propose a sequence of events describing
406 the evolution of the soil profile over time based on the Li isotope signatures.

407 ### 5.1 The role and fate of atmospheric inputs

408 The results presented above show that the Li/Cl ratio of rainfall and throughfall are higher
409 than the Li/Cl ratio in seawater (Figure 3) indicating that sea salts are not the only source of
410 Li in the rainwater. Other possible sources of Li to rainwater include the dissolution of
411 atmospheric dust or an anthropogenic source (Millot et al., 2010b). Influence of
412 anthropogenic Li can be discarded because of the absence of nuclear activity and fertilizers
413 in the National Park of Guadeloupe. Moreover, fertilizers are typically characterized by
414 extremely high δ^7Li (up to 215‰ determined by Negrel et al. (2009)) due to synthetic Li
415 additive derived from a ^{7}Li-rich reagent (Qi et al., 1997). As δ^7Li of Quiock rainwaters exhibit
416 a maximum value of +26.4‰, the additive source must have a Li signature lower than that of
417 seawater. Saharan dust and the remobilization of local and volcanic dusts from Montserrat
418 are therefore the best candidates to provide Li by leaching in the atmosphere followed by
419 deposition via rainfall. This is consistent with the pristine character of the Quiock Catchment.
420 The relationship between δ^7Li and Li/Na value in throughfall and stemflow (Figure 6a)
421 confirms that, at first order, Li in throughfall results from a mixture of sea salts and dissolved
422 mineral dust. Considering the scarcity of volcanic events able to spread andesite in the

atmosphere, the direction of the major winds and the high and regular flux of Saharan dusts reaching Guadeloupe (*i.e.* 100 $kg.ha^{-1}.yr^{-1}$), Saharan dusts are considered as the major additional source of Li to the rainwater. In order to calculate the proportion of Li from each source in the throughfall samples, we use Na as the best tracer for sea salt contribution in rainfall and throughfall (Keene et al., 1986; Negrel and Roy, 1998; Basak and Alagha, 2004; Rastogi and Sarin, 2005). Considering the seawater Li/Na ratio (Li/Na_{SW}), it is possible to calculate the proportion of sea salt Li (Li_{SW}) in rainwater and throughfall as follows:

$$Li_{SW} = Na_{TF} \times (\frac{Li}{Na})_{SW} \quad (4)$$

Where Na_{TF} is the concentration in the sample (throughfall or stemflow). In Figure 6b, the Li isotopic signature is plotted as a function of the proportion of Li coming from sea salts. The addition of Li from dusts is thus accompanied by a decrease in the Li isotopic signature. One peculiar data point exhibits a Li seawater proportion of 98% and a Li isotopic composition of +17.5‰, which may be related to the unusually (and unexplained) lower Na and Cl concentrations measured in this sample.

In order to calculate the Li mass balance at the catchment scale (see section 5.3), we assess the mean integrated δ^7Li value of throughfall because the mean δ^7Li of the individual samples might not be representative of the catchment integrated δ^7Li value due to the large variability and paucity of throughfall data. In order to assess this mean integrated δ^7Li value, we calculate the mean proportion of Li derived from sea salts in all throughfall samples collected (n=48) during our study with Equation (3). The mean proportion of Li in rain coming from sea salts is 75% with the remaining 25% derived from Saharan dust. We then compute the mean throughfall signature as a mixture between 25% of Saharan dust (δ^7Li_{SD} = -0.7‰) and 75% of sea salts (δ^7Li_{SS} = +31‰) assuming no fractionation of δ^7Li during mineral and sea salt dissolution. It is interesting to note that the calculated mean throughfall signature is +23.1‰, similar to the data reported by Millot et al. (2010b) for rainfall measured on the French Atlantic coast.

5.2 Using δ^7Li to interpret soil profile development

In the entire soil profile, the Li isotopic signature of the solid phase is low relative to andesite consistent with the preferential incorporation of ^6Li into secondary minerals during weathering processes. Figure 7 presents the Li isotopic signature of the soil as a function of τ_{Li}. As previously discussed (Section 4.2) at 15, 305, 488, 1219 and 1250 cm depths, the relatively high proportions of Li and other mobile elements (Figure 4), the higher primary mineral content (10% of quartz and microcline, Buss et al., 2010) and the Nd isotope signatures suggest that horizons of Saharan dust increase the local Li/Ti ratio at these depths. At 792 cm, we observe that the Ti concentration is abnormally low and thus, at this particular depth, the high Li/Ti ratio seems to be controlled by Ti depletion rather than by Li enrichment.

For soil samples, according to the behavior of Li isotopes during chemical weathering, the simplest hypothesis for the decrease in δ^7Li with depth is that the fractionation of Li isotopes is related to its depletion in the soil. Figure 7 shows that this is not the case as no relationship between τ_{Li} and the Li isotopic signature of the soil is observed (Figure 7). In Figure 7, we exclude samples impacted by dust deposition because their normalized Li content is not only derived from weathering processes but is also influenced by dust input or anomalous Ti concentrations. Most of the soil samples cluster around τ_{Li} = -0.6 while a very large decrease of the δ^7Li with depth is observed (from +3.9‰ at the top of the profile to -13.5‰ at depth). The -13.5‰ value of δ^7Li found at the base of the profile is one of the lowest values of δ^7Li in bulk soil ever published (Rudnick et al., 2004; Kisakurek et al., 2004; Huh et al., 2004; Liu et al., 2013).

A “batch” fractionation model similar to the one described in Bouchez et al. (2013) can be applied to interrogate the range of soil δ^7Li measured. This water-mineral interaction model, adapted from Johnson et al. (2004), considers that congruent dissolution of an initial rock leads to an initial solution (δ^7Li_{rock}) from which secondary phases precipitate. The model assumes an isotopic equilibrium between the residual solution (δ^7Li_{diss}) and the precipitated

475 solid phase (δ^7Li_{sec}). It is assumed that the main process fractionating Li isotopes is the
476 formation of secondary phases that preferentially incorporate ^6Li.

477 $$\delta^7 Li_{sec} = \frac{\alpha_{sec-diss} \times \delta^7 Li_{rock} + 1000\, f_{Li} \times (\alpha_{\mathrm{sec}\ -diss} - 1)}{\alpha_{sec-diss}\,(1 - f_{Li}) + f_{Li}} \quad (5)$$

478 The parameters of the model are the fractionation factor ($\alpha_{sec\text{-}diss}$) and the proportion of Li
479 incorporated into secondary phases ($1\text{-}f_{Li}$). $\alpha_{sec\text{-}diss}$ is expressed as follow:

480 $$\alpha_{\mathrm{sec}\ -diss} = \frac{\delta^7 Li_{sec} + 1000}{\delta^7 Li_{diss} + 1000} \quad (6)$$

481 $$1 - f_{Li} = \frac{(Li/Ti)_{sec}}{(Li/Ti)_{initial\ rock}} \quad (7)$$

482 In order to link the model with field data we make the following approximation:

483 $$1 - f_{Li} \approx -\tau_{Li} \quad (8)$$

484 This approximation assumes that the soil only contains secondary minerals, which is
485 reasonably consistent with the mineralogy of the soil samples (Buss et al., 2010). The
486 fraction of Li not incorporated into secondary minerals (f_{Li}) is fixed as the value measured in
487 the soil profile and we fit the fractionation factors ($\alpha_{sec\text{-}diss}$) needed to the soil profile data
488 (Figure 7).

489 The δ^7Li and the f_{Li} values of the deepest soil samples (having the most negative Li isotope
490 signature) can be modelled with a fractionation factor ($\alpha_{sec\text{-}diss}$) between 0.970 and 0.973, in
491 the low range of the fractionation factors in the literature (Li and West, 2014). Some authors
492 showed that $\alpha_{sec\text{-}diss}$ can vary depending on the nature of the secondary mineral formed. For
493 instance, Millot and Girard (2007) reported a $\Delta^7Li_{solution\text{-}rock}$ value of 7.1‰ for Li adsorption
494 onto kaolinite and a $\Delta^7Li_{solution\text{-}rock}$ value of 24.8‰ for gibbsite in agreement with values
495 reported by Pistiner and Henderson (2003). The fractionation factor values ($\alpha_{sec\text{-}diss}$ from
496 0.993 to 0.998) needed to fit the shallow profile data (Figure 7) are very low and not
497 consistent with literature values for the secondary minerals found in the Quiock profile.

Figure 7 shows that the batch equilibrium model provides a reasonable fit to the soil Li composition of the deeper part of the profile (610 cm to 1158 cm) with fractionation factors for gibbsite and kaolinite. However, the changes in $\alpha_{sec\text{-}diss}$ necessary to explain the δ^7Li variations along the profile are not consistent with the mineralogy, which is largely invariant with depth. Li and West (2014) have argued against a relationship between Li isotope fractionation factors and secondary phases. They propose instead that fractionation factors are linked to the mean annual temperature of a site. William and Hervig (2005) experiments suggested that high temperature Li fractionation by clays depended on crystal size. These results were obtained under simulated hydrothermal conditions (300°C and 100 MPa) which do not correspond to our conditions. There are no data on the influence of crystal size under supergene conditions and since the crystal size on site is unknown we cannot its influence.

The variation of δ^7Li in the profile could instead result from the surficial input of one or several additional Li sources with higher δ^7Li. The two possible candidates for this source of high δ^7Li are atmospheric (Saharan dust and seasalt) inputs and vegetation. The δ^7Li of Saharan dust is -0.7‰ and may vary in the upper continental crust signature range between 0 and +4‰ (Teng et al., 2004; Liu and Rudnick, 2011). It is clear that this source of Li is not sufficiently enriched in ^7Li to explain the isotopic signature of the upper part of the profile. Vegetation has a Li isotopic signature varying between +3.6 and +8.7 ‰ that could provide supplementary ^7Li to the soil (see Section 5.3). Organic carbon concentration in the soil profile (Lloret, 2010) indicates that less than 1g.kg^{-1} of organic matter is preserved in the soil lower than 20 cm depth. If we assume that the Li concentration is the same in both organic matter and vegetation, 1g kg^{-1} of organic matter corresponds to only 0.3 ppb of Li which is too low to influence the Li isotopic signature of the soil (approx. 5 ppm).

High soil δ^7Li values in the upper part of the profile can therefore only be explained by input of Li from throughfall that has a signature of around 23‰ and thus can provide a positive δ^7Li source to the soil profile. Such influence of atmospheric input on soil profiles has already been described in the literature for Li isotopes in Hawaii (Huh et al., 2004; Pistiner and

525 Henderson, 2003), in Iceland (Pogge von Strandmann et al., 2012), in South Carolina
526 (Rudnick et al., 2004, Teng et al., 2010) and for Mg isotopes in Puerto Rico (Chapela-Lara et
527 al., 2014). However, a recent study conducted in Hawaii states that atmospheric inputs of Li
528 do not impact solid soil (Ruy et al., 2014). Li isotope signatures in the Quiock profile suggest
529 that the Li of andesitic origin in the soil is progressively replaced by atmospheric Li, creating
530 a gradient of atmospheric influence from the top soil to the deep soil. The non-erratic
531 decrease of the soil Li isotopic signature from surface to deeper horizons is another evidence
532 for atmospheric Li diffusion coming from the surface.

533 To conclude, in the deeper soil away from atmospheric influence, Li isotope are a good proxy
534 for weathering degree of soils because in this highly weathered regime, Li depletion is
535 associated with very low δ^7Li (one of the lowest values reported in the literature) as a result
536 of intense weathering. However, at the surface, the influence of atmospheric inputs becomes
537 more and more important and soil samples have δ^7Li that mimics the source rock but are
538 depleted in Li compared to the source rock due to intense weathering. Therefore, surface soil
539 δ^7Li does not only reflect the high weathering degree (Li depletion) of soil samples as a
540 significant part of their Li is of marine origin. This shows that in environments characterized
541 by high precipitation rates and highly weathered soils, river suspended sediments sourced
542 from the erosion of top soil will have a Li depletion associated to a δ^7Li signature higher than
543 predicted value because of reincorporation of atmospheric lithium in secondary minerals.
544 This observation has important implications for using δ^7Li is solid weathering product as a
545 fingerprint for past weathering regimes. It also shows that at least for Li, chemical weathering
546 is not a simple mass loss of rock material but the result of an exchange with the atmosphere
547 (Bouchez and Gaillardet, 2014).

548 ### 5.3 Li budget at the catchment scale

549 #### 5.3.1 Li fluxes in the Quiock Creek catchment

550 Water and solid flux quantification and mean Li concentrations and isotopic compositions of
551 the different compartments, allow us to calculate the fluxes of Li that enter and leave the
552 Quiock Creek catchment. Taking into account the litter flux (7.8 t ha^{-1} yr^{-1}) and the Li
553 concentration in litter (0.3 ± 0.087 ppm), it is possible to determine the amount of Li provided
554 to the soil by vegetation decay (F_{VEG} = 18.7 ± 1.2 $g.yr^{-1}$) (Figure 8). This flux is relatively high
555 despite the fact that Li is not a plant nutrient and has no known physiological role. However
556 Rousteau (2014) showed that the vegetation is at steady-state with respect to carbon, *i.e.*,
557 the rate of carbon uptake is equal to the flux of carbon loss by vegetation. We hypothesize
558 that the organic Li sub-cycle is also at steady state. As the δ^7Li of vegetation is similar to that
559 of the soil solution, it appears that no fractionation occurs during Li uptake by vegetation.
560 Thus, we conclude that the litter flux does not influence the Li mass balance at the watershed
561 scale despite the flux of Li cycled through vegetation.

562 By combining the throughfall water flux (3079 mm over a surface of 8 ha) and its median Li
563 concentration (7 nmol L^{-1}) we calculate the total flux of dissolved atmospheric Li of 12.1 g Li
564 yr^{-1} (or 1724 mmol $Li.yr^{-1}$) (Figure 8). At the watershed scale, the dissolved yield of Li is 1.5 g
565 Li ha^{-1} yr^{-1}. The Li atmospheric flux in the Quiock Creek catchment is twice the value
566 measured in the volcanic Islands of La Réunion (Louvat et al., 1997) and of Azores
567 Archipelago (Pogge von Strandmann et al., 2010) which are both characterized by lower
568 precipitation rate. As 75% of the atmospheric flux to the Quiock Creek catchment comes
569 from sea salts, the sea salt input is F_{SS} = 9.1 g Li yr^{-1} and the remaining dissolved Li, derived
570 from leaching of the Saharan dust provides 3 g Li yr^{-1} (F_{SDdis}) (Figure 8). The flux of Saharan
571 dust that reaches the catchment is estimated to be 100 kg ha^{-1} yr^{-1} (Molinié, personal
572 communication). The Li concentration of the dust was measured as 18.5 ppm and thus
573 Saharan dust provides 14.8 g Li yr^{-1} (F_{SD}). Therefore, only a fifth of this flux (F_{SDd} = 3 $g\ Li.yr^{-1}$)
574 is dissolved in throughfall and the remainder reaches the soil in its solid form (F_{SDs} =11.8 g
575 $Li.yr^{-1}$). Depending on whether the particulate Li will be dissolved once deposited, we can

576 estimate that the input of Li from the atmosphere to the Quiock Creek watershed is between
577 12.1 g Li yr^{-1} (no dissolution of solid dust in the soil) to 23.9 g Li yr^{-1} (total dissolution of dust).

578 As the Quiock Creek water flux is 1130 mm over a surface area of 8 ha and the mean Li
579 concentration is 56 nmol L^{-1}, the dissolved Li flux at the outlet of the catchment is 5.1 mol Li
580 yr^{-1} or 35.7 g Li yr^{-1} (F_{QC}). The atmosphere contributes between 34% (no dissolution of solid
581 dust in the soil) and 67% (total dissolution of dust) of the Li exported, depending on the
582 atmospheric flux considered. These values are higher than those reported by Lemarchand et
583 al. (2010) and highlight the importance of Li atmospheric inputs in this environment.

584 5.3.2 Characterization of the weathering flux of Li

585 The calculated fluxes show that atmospheric inputs do not account for all of the Li exported.
586 The weathering flux (F_{wea}) and its isotopic composition (δ^7Li_{wea}) can be estimated using a box
587 model based on two assumptions:

588 - The catchment is at steady-state, consequently the input flux of Li to the catchment is
589 equal to the output Li flux and no Li is stored within the catchment.
590 - All the Li in this catchment is exported in a dissolved form. In other word, we neglect
591 the export of Li by suspended matter which has never been observed even during
592 flood events.

593 We consider two extreme scenarios in order to determine the lower and upper bounds for the
594 weathering fluxes of Li and for the Li isotopic signature of the weathering flux.

595 In the first scenario, we assume that the fraction of Li from the atmospheric dust that was not
596 dissolved during deposition (75% of the total dust input) can still contribute to an “internal”
597 source of Li to the soil solution and creek compartments (Hypothesis 1):

598 $$F_{SS} + F_{SD} + F_{wea} = F_{QC} \quad (9)$$

599 $$F_{SS}\,\delta^7Li_{SS} + F_{SD}\,\delta^7Li_{SD} + F_{wea}\,\delta^7Li_{wea} = F_{QC}\,\delta^7Li_{QC} \quad (10)$$

600 Where F_{SS} = 9.1 g Li yr^{-1} and F_{SD} = 14.8 g Li yr^{-1} are the Li inputs fluxes of sea salt and of
601 Saharan dust respectively. F_{QC} is the Li flux at the output of the catchment. δ^7Li_{SS}, δ^7Li_{SD} and
602 δ^7Li_{QC} are the Li isotopic signature of sea salts, Saharan dust and Quiock Creek respectively.
603 The resultant Li weathering flux, F_{wea} is 11.8 g Li yr^{-1} with an isotopic composition of 3.6‰.

604 In the second scenario we consider only the flux of dissolved Li that comes from the
605 throughfall as atmospheric input (Hypothesis 2):

606 $$F_{TF} + F_{wea} = F_{QC} \quad (11)$$

607 $$F_{TF}\ \delta^7Li_{TF} + F_{wea}\ \delta^7Li_{wea} = F_{QC}\ \delta^7Li_{QC} \quad (12)$$

608 F_{TF} and δ^7Li_{TF} are the flux and isotopic signature of throughfall. Here the resulting weathering
609 flux, F_{wea} of 23.6 g Li yr^{-1} with an isotopic composition of 1.4‰.

610 This exercise shows that the weathering flux of Li constitutes between 33% (Hypothesis 2)
611 and 66% (Hypothesis 1) of the Li exported at the outlet of the Quiock Creek catchment. The
612 isotopic composition of this Li weathering flux varies between 1.4‰ (Hypotheses 2) and
613 3.6‰ (Hypotheses 1). These signatures are not necessarily the signature of the solid phase
614 from which the Li originates. Indeed, the Li weathering flux (F_{wea}) is the combined result of
615 the flux of Li released by dissolution (D) of the lithogenic source and the flux of precipitation
616 (P) of Li-bearing secondary minerals (Figure 8). While dissolution does not fractionate Li
617 isotopes, precipitation of Li-bearing secondary minerals is accompanied by a fractionation
618 ($\Delta_{diss\text{-}sec}$). Thus we can write:

619 $$D - P = F_{wea} \quad (13)$$

620 $$D\ \delta^7Li_{LS} + P\ (\delta^7Li_{QC} - \Delta_{diss\text{-}sec}) = F_{wea}\ \delta^7Li_{wea} \quad (14)$$

621 Combining and rearranging these equations gives:

622 $$\delta^7Li_{LS} = ((F_{wea})\ \delta^7Li_{wea} - P\ (\delta^7Li_{QC} - \Delta_{diss\text{-}sec})) / (F_{wea}+P) \quad (15)$$

In these equations δ^7Li_{LS} is the Li isotopic signature of the lithogenic source of dissolved Li and varies between -13.5‰ (the most negative soil Li signature) and 5‰ (fresh andesite), which are the endmember values of materials at the site that could provide Li by weathering. $\Delta_{diss\text{-}sec}$ is set at 20‰ consistently to $\Delta_{diss\text{-}sec}$ values reported for similar context (Kisakurek et al., 2004 ; Rudnick et al., 2004 ; Dellinger et al., 2015). These calculations show that if P=0 (no precipitation of Li-bearing secondary minerals), then δ^7Li_{LS} is equal to δ^7Li_{wea}. If P>0, δ^7Li_{LS} is necessarily lower than δ^7Li_{wea} regardless of which hypothesis is taken into account. As δ^7Li_{wea} is lower than the andesite value, in any case δ^7Li_{LS} is lower than the andesite signature. The only lithological source of Li with a signature lower than andesite in the soil is secondary minerals. This result thus indicates secondary mineral dissolution occurs in the Quiock Creek catchment. This process has already been described in Guadeloupe for major elements and Mg isotopes (Dessert et al., 2015).

The main secondary mineral on site is the kaolinite ($Al_2Si_2O_5(OH)_4$) in which Li^+ in incorporated with Mg^+, both replacing Al^{3+} (Tardy et al., 1972). The dissolution constant of kaolinite regarding Al is $10^{-17.2}$ $mol_{Al}.cm^{-2}.s^{-1}$ (Carroll et al., 1988). Considering 10 m^2/g for the kaolinite specific surface, it corresponds to $10^{-4.7}$ $mol_{Al}.g_{(kaolinite)}^{-1}.an^{-1}$. We make the approximation that the soil is mostly composed by kaolinite. With a Li/Al ratio of 2.6 10^{-4} measured on site, it leads to 5.2 10^{-9} $mol_{Li}.g_{(kaolinite)}^{-1}.an^{-1}$. At Quiock Creek (8 ha), it signifies that the soil can at least release 29 g_{Li}/yr which is in very good agreement with the weathering Li flux measured on site (11.8 to 23.6 g_{Li}/an). This first order calculation supports the idea that secondary mineral dissolution occurs on Quiock Creek catchment, as shown by Li isotopes. Considering a mean weathering flux of 15 $g_{Li}.yr^{-1}$, it would take 400 000 years to deplete all the Li of the 10 m deep soil (which contains 6000 kg $_{Li}.ha^{-1}$).

As reported in Section 5.2, secondary minerals in the soil have incorporated Li derived from atmospheric inputs. Thus a primary part of the weathering flux comes from the atmosphere. This demonstrates that in a river draining highly weathered soils, even corrected for present-day atmospheric inputs, the weathering flux include elements of atmospheric origin.

650 Moreover it implies that processes involving Li isotopes cannot be simply envisaged as two
651 step processes (dissolution of parent rock without fractionation and precipitation of
652 secondary minerals with fractionation) but in some contexts it is important to integrate a third
653 process which is the dissolution of secondary minerals.

654 5.3.3 Implication for the use of Li isotopes as weathering proxy

655 The Quiock Creek watershed, characterized by thick soils, low physical erosion rate and high
656 chemical flux compared to physical erosion, is characteristic of a transport-limited context. In
657 an earlier study, Huh et al. (2001) proposed that this context is characterized by low isotopic
658 Li signature in the dissolved phase of rivers, as a consequence of equilibrium reactions
659 between water and clays. On the contrary, in weathering-limited settings (characterized by
660 thin soils and high physical erosion rate), Huh et al. (2001) proposed that dissolved load of
661 river exhibit high δ^7Li as a result of kinetic reactions. Later studies have shown that, in the
662 context of Iceland, the most weathering-limited context is associated with the lower δ^7Li
663 (Pogge von Strandmann et al., 2006; Vigier et al., 2009). In the present study, we found
664 particularly low Li isotopic signature associated with a transport-limited context. We explain
665 this observation by secondary mineral dissolution, which produces low isotopic Li signature.
666 The intermediate weathering regime, which is the most common context, leads to high δ^7Li
667 values (up to 36.2‰ in the Azores (Pogge von Strandmann et al., 2010) and to 30‰ in the
668 Columbia river basalt (Liu et al., 2015)). These observations in basaltic catchment, lead to a
669 bell-curved relationship between weathering regime and δ^7Li signature of dissolved load, as
670 proposed in Dellinger et al. (2015) for the Amazon Basin. In this bell-curved relationship,
671 lower δ^7Li are associated with extremely high and low weathering intensity while higher δ^7Li
672 are associated to intermediated weathering intensity (Dellinger et al., 2015).
673 Our study on the Quiock Creek catchment shows also that in a tropical context, despite the
674 high influence of atmospheric inputs (rich in heavy isotopes), the river exhibits a very low
675 δ^7Li. This observation is consistent with the model proposed by Wanner et al. (2014)

676 suggesting influence of secondary mineral dissolution to explain the lower values of δ^7Li in
677 the Cenozoic seawater.

678 Conclusion

679 In the Quiock Creek catchment, a large range of δ^7Li values is observed despite the small
680 scale of observation. Li isotopic composition varies from -13.5‰ in the deepest bulk soil
681 sample to +26.4‰ in throughfall water samples. This large range is explained by several
682 water-rock interaction processes.

683 Li and major element concentrations and Li isotopic compositions of throughfall samples
684 attest that sea salts are not the only source of Li in throughfall. At the first order, Li in
685 throughfall results from a mixture of Li derived from sea salts and Li derived from the
686 leaching of Saharan dust which is the main atmospheric terrestrial dust source to
687 Guadeloupe. It is therefore essential to characterize these atmospheric inputs to close the
688 mass balance at all scales of this catchment study.

689 Silicate weathering is usually considered to be the main source of Li in rivers but in the
690 Quiock Creek, atmospheric inputs account for 34 to 67% of Li exported at the outlet of the
691 catchment. These observations can be explained by the high precipitation rate and the
692 location of Guadeloupe in the Saharan dust corridor. In addition, the very high cation-
693 depleted soils are likely to provide a smaller amount of Li in comparison to less weathered
694 soils. Our work reinforces the need to accurately characterize the Li isotopic signature of
695 atmospheric inputs.

696 Nd isotopes combined with mineralogy and mobile element concentrations in the soil argue
697 for a multi- layered soil profile which has been built by successive volcaniclastic episodes,
698 separated by periods of dust deposition. Li isotopes are not affected by the multi-step soil
699 formation but rather by weathering processes in the soil. The high variability of δ^7Li in the soil
700 combined with the invariant Li content and the absence of mineralogical variation along the
701 soil profile attest to the incorporation of atmospheric Li into the bulk soil. The Li isotopic

composition decreases from the top to the bottom of the profile where atmospheric influence is probably minimal. In the deeper part of the profile (610-1250 cm), the isotopic fractionation factor is estimated to be between 0.970 and 0.973, consistent with values reported in the literature. In the shallower part of the profile (15-610 cm), a batch equilibrium model suggests that theoretical solution (calculated as in equilibrium with the present-day solid phase) is more influenced by atmospheric inputs compared to present-day soil solutions (sampled on site). Our results indicate that atmospheric inputs have had a significant influence on the soil formation. However, present-day soil solutions are more influenced by lithogenic Li than atmospheric inputs, implying that a change in the weathering regime has occurred between the past formation of the soil and the present day.

Despite the fact that Li is not a nutrient, the passive Li flux through vegetation is important. As vegetation does not seem to fractionate Li isotopes, this sub-cycle has little influence on the Li budget at the catchment scale.

The Li mass balance at the catchment scale highlights the importance of secondary mineral phase dissolution to solute export. Thus, in this highly weathered catchment, andesite does not participate in the weathering Li flux to the Quiock Creek.

Acknowledgements: This work has been financially supported by INSU-CNRS and by the Région Guadeloupe. H.L. Buss acknowledges support of the NSF-CZEN International Scholars Program. This work could not be done without logistical support from two INSU-CNRS observatories run by IPGP: the Observatoire Volcanologique et Sismologique de Guadeloupe (OVSG) and the Observatoire de l'Eau et de l'Erosion aux Antilles (ObsErA). We thank in particular O. Crispi from OVSG for his assistance in field work and the ObsErA advisor E. Lajeunesse. This study also received funding from Région Guadeloupe which supported the project "Vulnerability of tropical ecosystems of Guadeloupe", in partnership with the Antilles-Guyane University and the Parc National de Guadeloupe. We especially

728 want to thank A. Rousteau and staff of the Parc National for field assistance. X. Quidelleur
729 and P. Lahitte (Paris Sud 11 University) are also thanked for having provided us rock sample
730 from Guadeloupe. Major element concentrations were measured by L. Cordier and C. Gorge.
731 Thanks are extended to A. Michel, M. Tharaud, B. Villemant, B. Caron, J. Moureau and P.
732 Louvat for their analytical assistance. This study greatly benefited from comments from S.
733 Henchiri, J. Bouchez, G. Carazzo, A. Rousteau, M. Dulormne, F. Bussière, J. Molinié, R.
734 Losno and J.C. Komorowski. We also thank Philip Pogge von Strandmann, an anonymous
735 reviewer and editor Jeremy Fein for suggestions that greatly improved this manuscript.

736

737 Basak B., Alagha B. (2004) The chemical composition of rainwater over Buyukcekmece
738 Lake, Istanbul. *Atmospheric Research* **71**, (4) 275-288

739 Berner R.A. (1995) Chemical weathering and its effect on atmospheric CO2 and climate.
740 Chemical weathering rates of silicate minerals. *Reviews in mineralogy* **31**, 565-588

741 Borg L.E. and Banner J.L. (1996) Neodymium and strontium isotopic constraints on soil
742 sources in Barbados, West Indies. *Geochimica et Cosmochimica Acta* **60** (21) 4193-4206

743 Bouchez J., von Blanckenburg F., Schuessler J. A. (2013) Modeling novel stable isotope
744 ratios in the weathering zone. *AmericanJournal of Science* **313**, (4) 267–308

745 Boudon G., Dagain J., Semet M. P., Westercamp D. (1988) Le massif volcanique de la
746 Soufrière (département de la Guadeloupe, Petites Antilles). In: BRGM (Ed.), Carte
747 géologique au 1/20.000ème

748 Brimhall G.H. and Dietrich W.E. (1987) Constitutive mass balance relations between
749 chemical composition, volume, density, porosity, and strain in metasomatic hydrochemical
750 systems: results on weathering and pedogenesis. *Geochimica et Cosmochimica Acta* **51**,
751 567–587

752 Burton K., Vigier N. (2011) Lithium isotopes as tracers in marine and terrestrial
753 environments. *Handbook of Environmental Isotope Geochemistry*, 41–59

754 Buss H.L., White A.F., Dessert C., Gaillardet J., Blum A.E., Sak P.B. (2010) Depth profiles in
755 a tropical volcanic critical zone observatory: Basse-Terre, Guadeloupe. In: Torres-Alvarado,
756 I.S., Birkkle, P. (Eds.), Proceedings of the 13th International conference on water-Rock
757 Interaction. Taylor & Francis Group, London, UK

758 Caro G., Bourdon B., Birck J. L., & Moorbath S. (2006) High-precision $^{142}Nd/^{144}Nd$
759 measurements in terrestrial rocks: constraints on the early differentiation of the Earth's
760 mantle. *Geochimica et Cosmochimica Acta* **70**(1), 164-191

761 Carroll-Webb, S. A., & Walther, J. V. (1988) A surface complex reaction model for the pH-
762 dependence of corundum and kaolinite dissolution rates. *Geochimica et Cosmochimica Acta*
763 **52**(11), 2609-2623

764 Chapela-Lara M., Buss H. L., von Strandmann P. A. P., Dessert C., & Gaillardet J. (2014)
765 Controls on the Mg cycle in the tropics: insights from a case study at the Luquillo Critical
766 Zone Observatory. *Procedia Earth and Planetary Science* **10**, 200-203

767 Colmet-Daage F. and Bernard Z. (1979) Contribution à l'Atlas des départements d'Outre-
768 mer: Guadeloupe. Carte des sols de la Guadeloupe, Grande-Terre, Marie-Galante. Carte
769 des pentes et du modelé de la Guadeloupe, Grande-Terre, Marie-Galante. ORSTOM,
770 Antilles

771 Dellinger M., Gaillardet J., Bouchez J., Calmels D., Galy V., Hilton R. G., Louvat P., France-
772 Lanord C. (2014) Lithium isotopes in large rivers reveal the cannibalistic nature of modern
773 continental weathering and erosion. *Earth and Planetary Science Letters* **401**, 359–372

774 Dellinger M., Gaillardet J., Bouchez J., Calmels D., Louvat P., Dosseto A., Gorge C., Maurice
775 L. (2015) Riverine Li isotope fractionation in the Amazon River basin controlled by the
776 weathering regimes. *Geochimica et Cosmochimica Acta* **164**, 71-96

777 Dellinger M., (2013) Apport des isotopes du lithium et des éléments alcalins à la
778 comprehension des processus d'altération chimique et de recyclage sédimentaire PhD
779 Thesis. Institut de Physique du Globe de Paris

780 Dessert C., Lajeunesse E., Lloret E., Clergue C., Crispi O., Capmas F., Gorge C., Quidelleur,
781 X. (2015) Controls on chemical weathering intensity in volcanic mountainous tropical island,
782 Guadeloupe (FWI) Accepted to *Geochimica et Cosmochimica Acta*

783 Flesch G., Anderson Jr, A., Svec H. (1973) A secondary isotopic standard for 6Li/7Li
784 determinations. *International Journal of Mass Spectrometry and Ion Physics* **12** (3), 265–272

785 Gaillardet J., Rad S., Rivé K., Louvat P., Gorge C., Allègre C.-J., Lajeunesse E. (2011)
786 Orography-driven chemical denudation in the Lesser Antilles: evidence for a new feed-back
787 mechanism stabilizing atmospheric CO2. *American Journal of Science* **311**, 851–894

788 Glaccum R.A., Prospero J.M. (1980) Saharan aerosols over the tropical north atlantic-
789 mineralogy. *Marine Geology* **37**, 295-321

790 Halama R., Savov I.P., Rudnick R.L. (2009) Insights into Li and Li isotope cycling and sub-
791 arc metasomatism from veined mantle xenolith, Kamchatka. *Contributions to Mineralogy and*
792 *Petrology* **158**, 197-22

793 Henchiri S., Clergue C., Dellinger M., Gaillardet J., Louvat P., Bouchez J. (2014) The
794 influence of hydrothermal activity on the Li isotopic signature of rivers draining volcanic
795 areas. *Procedia Earth and Planetary Science* **10**, 223–230

796 Herwitz S. R., Muhs D. R., Prospero J. M., Mahan S. and Vaughn B. (1996) Origin of
797 Bermuda's clay-rich Quaternary paleosols and their paleoclimatic significance. *Journal of*
798 *Geophysical Research: Atmospheres* **101**, 23389–23400

799 Huang K. E., You C. F., Liu Y. H., Wang R. M., Lin P. Y., Chung C. H. (2010) Low-memory,
800 small sample size, accurate and high-precision determinations of lithium isotopic ratios in
801 natural materials by MC-ICP-MS. *Journal of Analytical Atomic Spectrometry* **25**, 1019–1024

802 Huh Y., Chan L., Zhang L., Edmond J. (1998) Lithium and its isotopes in major world rivers:
803 implications for weathering and the oceanic budget. *Geochimica et Cosmochimica Acta* **62**,
804 (12) 2039–2051

805 Huh Y., Chan L., Edmond J. (2001) Lithium isotopes as a probe of weathering processes:
806 Orinoco River. *Earth and Planetary Science Letters* **194**, (1-2) 189–199

807 Huh Y., Chan L., Chadwick O.A. (2004) Behavior of lithium and its isotopes during
808 weathering of Hawaiian basalt. *Geochemistry, Geophysics, Geosystems* **5**, (9) 1-22

809 James R. H., Palmer M. R. (2000) The lithium isotope composition of international rock
810 standards. *Chemical Geology* **166**, (3) 319–326

811 Jeffcoate A.B., Elliott T., Thomas A., Bouman C. (2007) Precise/small sample size
812 determination of lithium isotopes composition of geological reference materials and modern
813 seawater by MC-ICP-MS. *Geostandard and Geoanalytical Research* **28** (1), 161-172

814 Johnson C. M., Beard B. L., Albarède F., Union C. G. (2004) Geochemistry of nontraditional
815 stable isotopes. *Mineralogical Society of America* Washington, DC

816 Keene W.C., Pszenny A.A.P., Galloway J., Hawley M.E. (1986) Sea-salt corrections and
817 interpretation of constituent ratios in marine precipitation. *Journal of Geophysical Research*
818 **91**, 6647–6658

819 Kisakurek B, Widdowson M., James RH. (2004) Behaviour of Li isotopes during continental
820 weathering: the Bidar laterite profile, India. *Chemical Geology* **212**, 27-44

821 Kisakurek B., James R., Harris N. (2005) Li and δ^7Li in Himalayan Rivers: Proxies for silicate
822 weathering? *Earth and Planetary Science Letters* **237**, (3-4) 387–401

823 Lemarchand E., Chabaux F., Vigier N., Millot R., Pierret M. (2010) Lithium isotope
824 systematics in a forested granitic catchment (Strengbach, Vosges Mountains, France).
825 *Geochimica et Cosmochimica Acta* **74** (16), 4612–4628

826 Li G., West A. J. (2014) Evolution of cenozoic seawater lithium isotopes: Coupling of global
827 denudation regime and shifting seawater sinks. *Earth and Planetary Science Letters* **401**,
828 284–293

829 Liu X-M., Rudnick R.L. (2011) Constraints on continental crustal mass loss via chemical
830 weathering using lithium and its isotopes. *Proceedings of the National Academy of Sciences*
831 **108**, (52) 20873-20880

832 Liu X-M., Rudnick R.L., McDonough W.F., Cummings M.L. (2013) Influence of chemical
833 weathering on the composition of the continental crust: Insights from Li and Nb isotopes in
834 bauxite profiles developed on Columbia River Basalts. *Geochimica et Cosmochimica Acta*
835 **115**, 73-91

836 Liu, X. M., Wanner, C., Rudnick, R. L., & McDonough, W. F. (2015) Processes controlling
837 δ^7Li in rivers illuminated by study of streams and groundwaters draining basalts. *Earth and*
838 *Planetary Science Letters* **409**, 212-224

839 Lloret E., Dessert C., Gaillardet J., Albéric P., Crispi O., Chaduteau C., Benedetti M. (2011)
840 Comparison of dissolved inorganic and organic carbon yields and fluxes in the watersheds of
841 tropical volcanic islands, examples from Guadeloupe (French West Indies). *Chemical*
842 *Geology* **280**, 65-78

843 Lloret E., Dessert C., Pastor L., Lajeunesse E., Crispi O., Gaillardet J. and Benedetti M.
844 (2013) Dynamic of particulate and dissolved organic carbon in small volcanic mountainous
845 tropical watersheds. *Chemical Geology* **351**, 229-244

846 Lloret E. (2010) Dynamique du carbone dans des petits bassins versants tropicaux, Exemple
847 de la Guadeloupe. phD Thesis. Université Paris Diderot

Loescher H.W., Gholz H.L., Jacobs J.M., Oberbauer S.F. (2005) Energy dynamics and modeled evapotranspiration from a wet tropical forest in Costa Rica. *Journal of Hydrology* **315**, 274-294

Ma L., Chabaux F., Pelt E., Granet M., Sak P.B., Gaillardet J., Lebedeva M., Brantley S.L. (2012) The effect of curvature on weathering rind formation : Evidence from Uranium-series isotopes in basaltic andesite weathering clast in Guadeloupe. *Geochimica et Cosmochimica Acta* **80**, 92-107

Magna T., Wiechert U., Grove T.L., Halliday A.N. (2006) Lithium isotope fractionation in the southern Cascadia subduction zone. *Earth and Planetary Science Letters* **250**, 428-443

Mahowald N. M., Muhs D. R., Levis S., Rasch P. J., Yoshioka M., Zender C. S., Luo C. (2006) Change in atmospheric mineral aerosols in response to climate: Last glacial period, pre-industrial, modern, and doubled carbon dioxide climates. *Journal of Geophysical Research: Atmospheres* **111** (D10)

Millot R., Guerrot C., Vigier N. (2004) Accurate and High-Precision Measurement of Lithium Isotopes in Two reference Materials by MC-ICP-MS. *Geostandards and Geoanalytical Research* **28**, (1) 153–159

Millot R., Girard J. (2007) Lithium isotope fractionation during adsorption onto mineral surfaces. In: International Meeting on Clays in Natural & Engineered Barriers for Radioactive Waste Confinement, Lille, France

Millot R., Gaillardet J. (2010a). Behaviour of lithium and its isotopes during weathering in the Mackenzie Basin, Canada. *Geochimica et Cosmochimica Acta* **67**, 1305-1329

Millot R, Petelet-Giraud E., Guerrot C., Negrel P. (2010b) Multi-isotopic composition (δ^7Li- δ 11B- δD- δ^{18}O) of rainwaters in France: Origin and spatio-temporal characterization. *Applied Geochemistry* **25**, 1510-1524

Misra S., Froelich P. (2012) Lithium isotope history of cenozoic seawater : Changes in silicate weathering and reverse weathering. *Science* **335**, (6070) 818–823

Moreno T., Querol X., Castillo S., Alastuey A., Cuevas E., Herrmann L., Mounkaila M., Elvira J., Gibbons W. (2006) Geochemical variations in aeolian mineral particles from the Sahara–Sahel Dust Corridor. *Chemosphere* **65** 261-270

Muhs D.R. and Budahn J.R. (2009) Geochemical evidence for African dust and volcanic ash inputs to terra rossa soils on carbonate reef terraces, northern Jamaica, West Indies. *Quaternary International* **196** 13–35

Négrel Ph., Roy S. (1998) Chemistry of rainwater in the Massif Central (France): a strontium isotope and major element study. *Applied Geochemistry.* **13**, 941–952

Négrel Ph., Millot R., Brenot A. (2009) Lithium isotopes as a probe of groundwater circulation in a peat land. In: 8th International Symposium on Applied Isotope Geochemistry, La Malbaie, Canada.

885 Opfergelt S., Georg R.B., Delvaux B., Cabidoche Y.-M., Burton K.W., Halliday A.N. (2012)
886 Mechanisms of magnesium isotope fractionation in volcanic soil weathering sequences,
887 Guadeloupe. *Earth and Planetary Science Letters* **341-344**, 176-185

888 Penniston-Dorland S.C., Bebout G.E., Pogge von Strandmann P.A.E., Elliott T., Sorensen
889 S.S. (2012) Lithium and its isotopes as tracers of subduction zone fluids and metasomatic
890 processes: Evidence from the Catalina Schist, California, USA. *Geochimica et*
891 *Cosmochimica Acta* **77** 530–545

892 Pett-Ridge J.C., Derry L.A., Kurtz A.C. (2009) Sr isotopes as a tracer of weathering
893 processes and dust inputs in a tropical granitoid watershed, Luquillo Mountains, Puerto Rico.
894 *Geochimica et Cosmochimica Acta* **73** 25-43

895 Pistiner J., Henderson G. (2003) Lithium-isotope fractionation during continental weathering
896 processes. *Earth and Planetary Science Letters* **214**, (1) 327–339

897 Pogge von Strandmann, P. A, Burton, K. W., James, R. H., van Calsteren, P., Gíslason, S.
898 R., & Mokadem, F. (2006) Riverine behaviour of uranium and lithium isotopes in an actively
899 glaciated basaltic terrain. *Earth and Planetary Science Letters* **251**(1), 134-147

900 Pogge von Strandmann, P. A., Burton, K. W., James, R. H., van Calsteren, P., & Gislason, S.
901 R. (2010) Assessing the role of climate on uranium and lithium isotope behaviour in rivers
902 draining a basaltic terrain. *Chemical Geology* **270**(1), 227-239

903 Pogge von Strandmann P. A., Opfergelt S., Lai Y.-J., Sigfússon B., Gislason S. R., Burton K.
904 W. (2012) Lithium, magnesium and silicon isotope behaviour accompanying weathering in a
905 basaltic soil and pore water profile in Iceland. *Earth and Planetary Science Letters* **339**, 11–
906 23

907 Pogge von Strandmann, P. A. & Henderson, G. M. (2015) The Li isotope response to
908 mountain uplift. *Geology* **43**(1), 67-70

909 Prospero J. M., Bonatti E., Schubert C. and Carlson T. N. (1970) Dust in Caribbean
910 atmosphere traced to an African dust storm. *Earth and Planetary Science Letters* **9**, 287–290

911 Qi H.P., Taylor P.D.P., Berglund M., De Bièvre P. (1997) Calibrate measurements of the
912 isotopic composition and atomic weight of the natural reference material IRMM-016.
913 *International Journal of Mass Spectrometry and Ion Processes* **171**, 263-268

914 Qi H. P., Coplen T. B., Wang Q. Z., & Wang Y. H. (1997) Unnatural isotopic composition of
915 lithium reagents. *Analytical chemistry* **69**(19), 4076-4078

916 Rad S., Louvat P., Gorge C., Gaillardet J., Allègre C.J. (2006) River dissolved and solid
917 loads in the Lesser Antilles: New insight into basalt weathering processes. *Journal of*
918 *Geochemical Exploration* **88**, 308– 312

919 Rad, S., Rivé, K., Vittecoq, B., Cerdan, O., & Allègre, C. J. (2013) Chemical weathering and
920 erosion rates in the Lesser Antilles: An overview in Guadeloupe, Martinique and Dominica.
921 *Journal of South American Earth Sciences* **45**, 331-344

Rastogi N., Sarin M.M. (2005) Chemical characteristics of individual rain events from a semi-arid region in India: three-year study. *Atmospheric Environment* **39**, 3313–3323

Richard P., Shimizu N., & Allègre C. J. (1976). ^{143} Nd/^{146} Nd, a natural tracer: an application to oceanic basalts. *Earth and Planetary Science Letters* **31**(2), 269-278

Roche M.A (1982) Evapotranspiration réelle de la forêt amazonienne en Guyane. *Cah. ORSTOM, série Hydrologie* **14**, (1) 37-44

Rosner M., Ball L., Peucker-Ehrenbrink B., Blusztajn J., Bach W., Erzinger J. (2007) A simplified, accurate and fast method for lithium isotope analysis of rocks and fluids, and _7li values of seawater and rock reference materials. *Geostandards and Geoanalytical Research* **31** (2), 77–88

Rousteau A., Portecop J. and Rollet B. (1994) Carte écologique de la Guadeloupe. Université Antilles Guyane, ONF, Conseil Général, Parc National de la Guadeloupe, Guadeloupe.

Rousteau A., Dessert C., Dulormne M. (2014) Bilan des travaux réalisés dans le cadre du projet « Vulnérabilité des écosystèmes insulaires guadeloupéens aux changements climatiques » - Région Guadeloupe funding

Rudnick R.L., Tomascak P.B., Njo H.B., Gardner L.R. (2004) Extreme lithium isotopic fractionation during continental weathering revealed in saprolites from South Carolina. *Chemical Geology* **212**, 45-57

Ruy J., Vigier N., Lee S., Lee K., Chadwick O.A. (2014) Variation of lithium isotope geochemistry during basalt weathering and secondary mineral transformations in Hawaii *Geochimica et Cosmochimica Acta* **145**, 103–115

Sak P. B., Navarre-Stichler A. K., Miller C. E., Daniel C. C., Gaillardet J., Buss H. L., Lebedeva M. I. and Brantley S. L. (2010) Controls on rind thickness on basaltic andesite clasts weathering in Guadeloupe. *Chemical Geology* **276**, 129-143

Samper A., Quidelleur X., Lahitte P. and Mollex D. (2007) Timing of effusive volcanism and collapse events within an oceanic arc island: Basse-Terre, Guadeloupe archipelago (Lesser Antilles Arc). *Earth and Planetary Science Letters* **258**, 175-191

Schellekens J., Bruijnzeel L.A., Scatena F.N., Bink N.J., Holwerda F., 2000. Evaporation from a tropical rain forest, Luquillo Experimental Forest, eastern Puerto Rico. *Water Resources Research* **36**, (8) 2183–2196

Schuessler J. A., Schoenberg R., Sigmarsson O., 2009. Iron and lithium isotope systematics of the Hekla volcano, Iceland-evidence for Fe isotope fractionation during magma differentiation. *Chemical Geology* **258**, (1) 78–91

Schluz M.S. and White A.F., 1999. Chemical weathering in a tropical watershed, Luquillo Mountains, Puerto Rico III : Quartz dissolution rates. *Geochimica et Cosmochimica Acta* **63**, 337-350.

959 Tardy, Y., Krempp, G., & Trauth, N. (1972) Le lithium dans les minéraux argileux des
960 sédiments et des sols. *Geochimica et Cosmochimica Acta* **36**(4), 397-412

961 Teng F.Z., McDonough W.F., Rudnick R.L., Dalpé C., Tomascak P.B., Chappell B.W., Gao
962 S. (2004) Lithium isotopic composition and concentration of the upper continental crust.
963 *Geochimica et Cosmochimica Acta* **68**, 4167-4178

964 Teng, F. Z., Li, W. Y., Rudnick, R. L., & Gardner, L. R. (2010) Contrasting lithium and
965 magnesium isotope fractionation during continental weathering. *Earth and Planetary Science*
966 *Letters* **300**(1), 63-71

967 Tomascak P.B., Hemming N.G., Hemming S.R., (2003) The lithium isotopic composition of
968 waters of the Mono Basin, California. *Geochimica et Cosmochimica Acta* **67**, (4) 601–611

969 Trapp J.M., Millero F.J., and Prospero J.M. (2010) Temporal variability of the elemental
970 composition of African dust measured in trade wind aerosols at Bardados and Miami. *Marine*
971 *Chemistry* **120**, 71-82

972 Vetter J. (2005) Lithium content of some common edible wild-growing mushrooms. *Food*
973 *Chemistry* **90**, 31–37

974 Vigier N., Decarreau A., Millot R., Carignan J., Petit S., France-Lanord C. (2008) Quantifying
975 Li isotope fractionation during smectite formation and implications for the Li cycle.
976 *Geochimica et Cosmochimica Acta* **72**, (3) 780–792

977 Vigier N., Gislason S., Burton K., Millot R., Mokadem F. (2009) The relationship between
978 riverine lithium isotope composition and silicate weathering rates in Iceland. *Earth and*
979 *Planetary Science Letters* **287**, (3) 434–441

980 Vigier, N., & Goddéris, Y. (2015) A new approach for modeling Cenozoic oceanic lithium
981 isotope paleo-variations: the key role of climate. *Climate of the Past* **11**(4), 635-645

982 Vlastélic I., Koga K., Chauvel C., Jacques G., Télouk P. (2009) Survival of lithium isotopic
983 heterogeneities in the mantle supported by HIMU-lavas from Rurutu Island, Austral Chain.
984 *Earth and Planetary Science Letters* **286**, (3) 456–466

985 Walker J., Hays P., Kasting J. (1981) A negative feedback mechanism for the long-term
986 stabilization of the Earth's surface temperature. *Journal of Geophysical Research.* **86**, (C10)
987 9776–9782

988 Wang, Q. L., Chetelat, B., Zhao, Z. Q., Ding, H., Li, S. L., Wang, B. L., ... & Liu, X. L. (2015)
989 Behavior of lithium isotopes in the Changjiang River system: Sources effects and response
990 to weathering and erosion. *Geochimica et Cosmochimica Acta* **151**, 117-132

991 Wanner, C., Sonnenthal, E. L., & Liu, X. M. (2014) Seawater δ^7Li: A direct proxy for global
992 CO 2 consumption by continental silicate weathering? *Chemical Geology* **381**, 154-167

993 Weaver P.L., Murphy P.G. (1990). Forest Structure and Productivity in Puerto Rico's Luquillo
994 Mountains. *Biotropica* **22**, (1) 69-82

995 Widory D., Petelet-Giraud E., Négrel Ph., Ladouche B. (2005). Tracking the sources of
996 nitrate in groundwater using coupled nitrogen and boron isotopes: a synthesis.
997 *Environmental Science and Technology* **39**, 539–548

998 Williams, L. B., & Hervig, R. L. (2005) Lithium and boron isotopes in illite-smectite: the
999 importance of crystal size. *Geochimica et Cosmochimica Acta* **69**(24), 5705-5716

1000 Wimpenny, J., James, R. H., Burton, K. W., Gannoun, A., Mokadem, F., & Gíslason, S. R.
1001 (2010a) Glacial effects on weathering processes: new insights from the elemental and lithium
1002 isotopic composition of West Greenland rivers. *Earth and Planetary Science Letters* **290**(3),
1003 427-437

1004 Wimpenny J., Gíslason S.R., James R.H., Gannoun A., Pogge Von Strandmann P.A.E. and
1005 Burton K.W. (2010b) The behaviour of Li and Mg isotopes during primary phase dissolution
1006 and secondary mineral formation in basalt. *Geochimica et Cosmochimica Acta* **74**, 5259–
1007 5279

1008 Witherow, R. A., Lyons, W. B., & Henderson, G. M. (2010) Lithium isotopic composition of
1009 the McMurdo Dry Valleys aquatic systems. *Chemical Geology* **275**(3), 139-147

1010 Zahibo N., Pelinovsky E., Talipova T., Rabinovich A., Kurkin A., and Nikolkina I. (2007)
1011 Statistical analysis of cyclone hazard for Guadeloupe, Lesser Antilles. *Atmospheric Research*
1012 **84**, 13-29

1013

Figures captions:

Figure 1: The Quiock Creek catchment (16°17'N, 61°7 0'W) in the National Park of Guadeloupe. SS : soil solutions, TF : throughfall and SF : stemflow. The soil profile was sampled during lysimeter installation. The rain gauge is located in a clearing on the roof of the "Maison de la forêt".

Figure 2: Cl concentrations (µmol L^{-1}) plotted as a function of Na concentrations (µmol L^{-1}) in rainwater samples (RF) collected on site (RF-MF) and at the OVSG (RF-OVSG), and in throughfall (TF) samples. The seawater dilution line (dashed) and the linear regression line (solid) between Na and Cl for throughfall samples are shown.

Figure 3: Li/Cl molar ratios for throughfall, rainfall, Quiock Creek and soil solution samples. The dashed line represents the sea water Li/Cl ratio.

Figure 4: Mass transfer coefficients (τ) for Li and major elements (a.) and Li/Na wt. ratios (b.) in soil samples as functions of depth relative to andesite. τ is calculated considering Ti to be immobile (Square for Li, black diamond for Mg, triangle for K, black point for Na and open diamonds for Ca). εNd (c.) of the bulk soil and quartz + feldspar content (d.) are also shown.

Figure 5: Lithium isotopic compositions measured in all compartments of the Quiock Creek catchment. Error bars, smaller than 0.5‰, are contained in the data points.

Figure 6: δ^7Li plotted as a function of the Li/Na molar ratio in throughfall and stemflow samples. The star represents the sea salt signature. Andesite and Saharan dust signatures are also shown. 6b: Li isotopic compositions plotted as a function of the proportion of Li coming from marine sea salts in throughfalls samples. The sea water isotopic composition is also shown.

Figure 7: Li isotopic composition of soil samples as a function of τ_{Li}. Straight lines represent the evolution of δ^7Li vs τ_{Li} predicted by the batch equilibrium model. The depth for each soil sample is indicated.

Figure 8: Fluxes of Li and Li isotopic compositions of compartments in the Quiock Creek catchment. Fluxes, indicated in italics, were measured on site. Sea salt flux (F_{SS}) and flux of Saharan dust dissolved in throughfall (F_{SDd}) were calculated from the chemical composition of throughfall (Section 5.1). The Saharan dust flux that reaches the soil in the solid phase (F_{SDs}) is also calculated in Section 5.1. Fluxes in red are computed with a steady state box model in Section 5.3. δ^7Li_{wea} is the isotopic signature of the weathering flux (F_{wea}). The weathering flux can be divided in two fluxes: the dissolution Li flux (D) of the lithogenic source of Li (δ^7Li_{LS}) and the precipitation flux (P) which is accompanied by fractionation (Δ).

Figure1

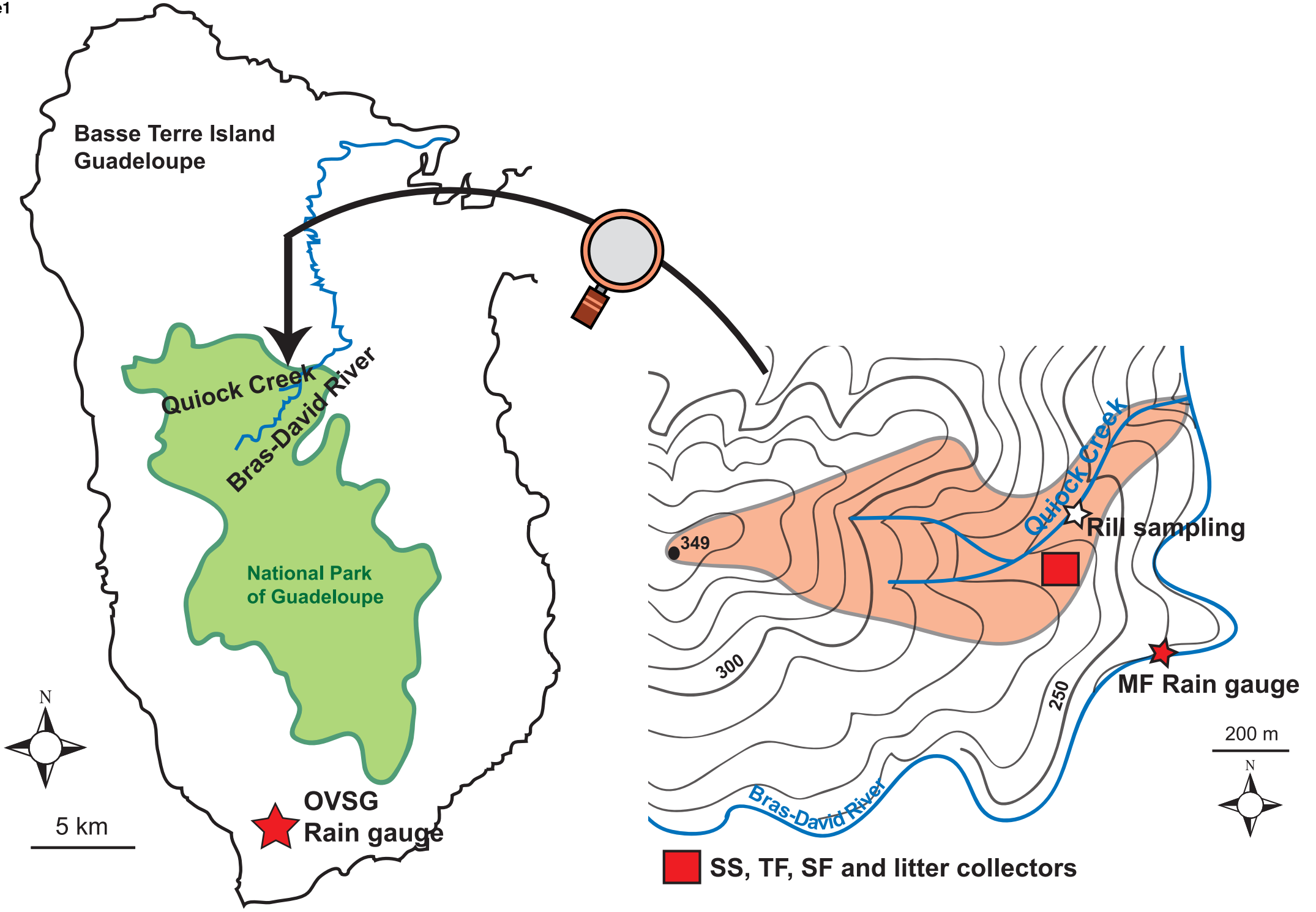
Basse Terre Island
Guadeloupe
Quiock Creek
Bras-David River
National Park
of Guadeloupe
N
5 km
OVSG
Rain gauge
349
300
250
Quiock Creek
Rill sampling
MF Rain gauge
200 m
N
Bras-David River
SS, TF, SF and litter collectors

Figure2

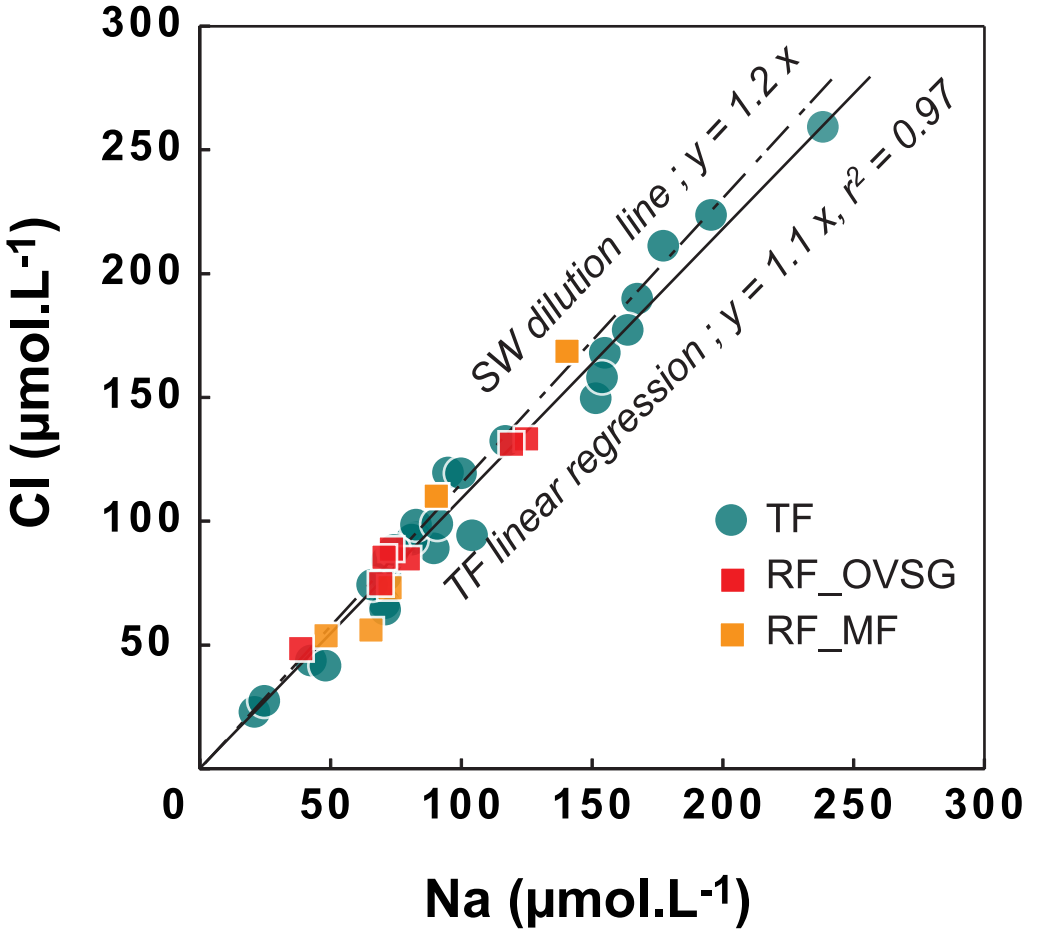
300
250
200
150
100
50
0
50
100
150
200
250
300
Cl (µmol.L-1)
Na (µmol.L-1)
SW dilution line ; y = 1.2 x
TF linear regression ; y = 1.1 x, r2 = 0.97
TF
RF_OVSG
RF_MF

Figure3

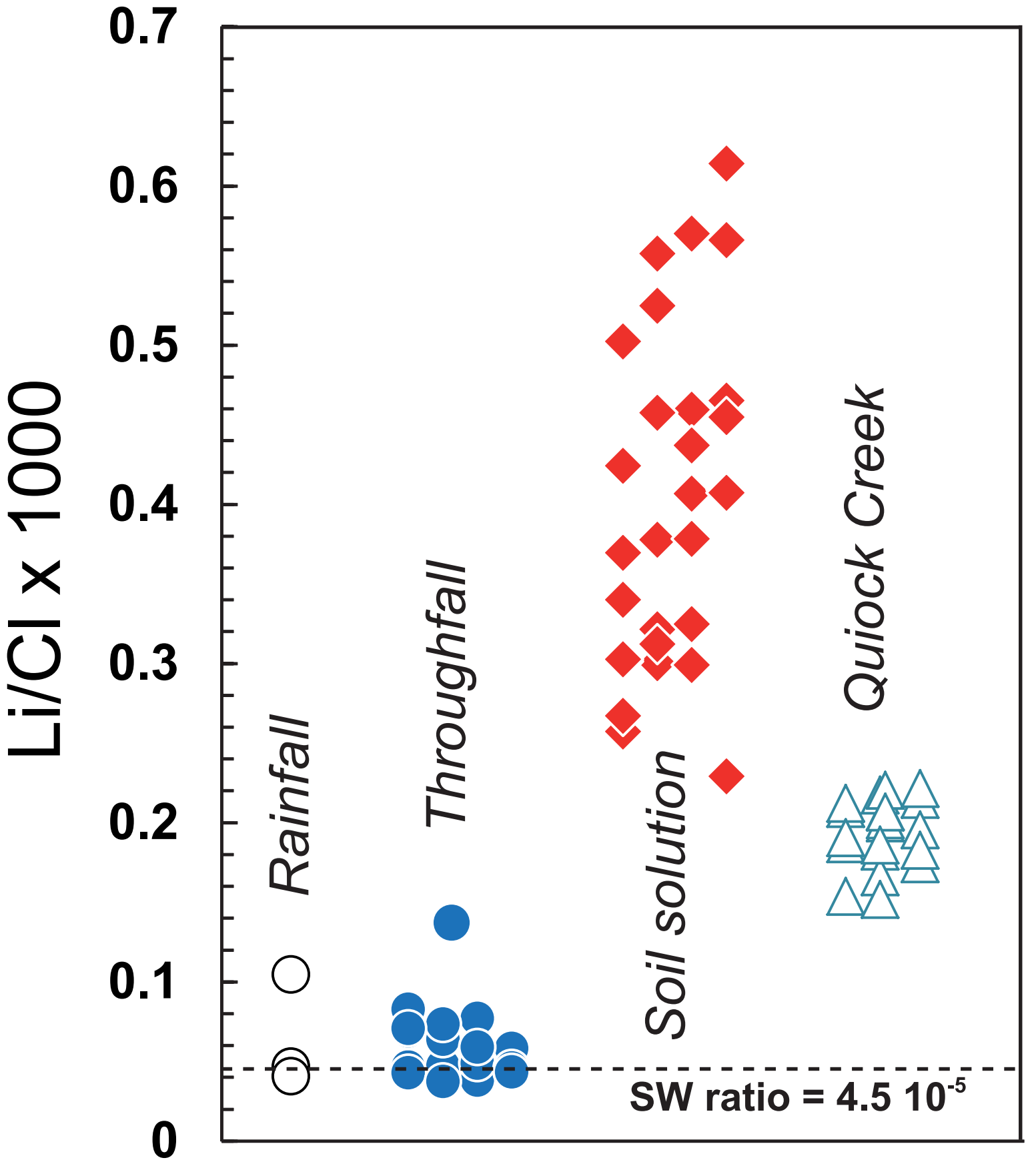
Li/Cl x 1000
0.7
0.6
0.5
0.4
0.3
0.2
0.1
0
Rainfall
Throughfall
Soil solution
Quiock Creek
SW ratio = 4.5 10-5

Figure4

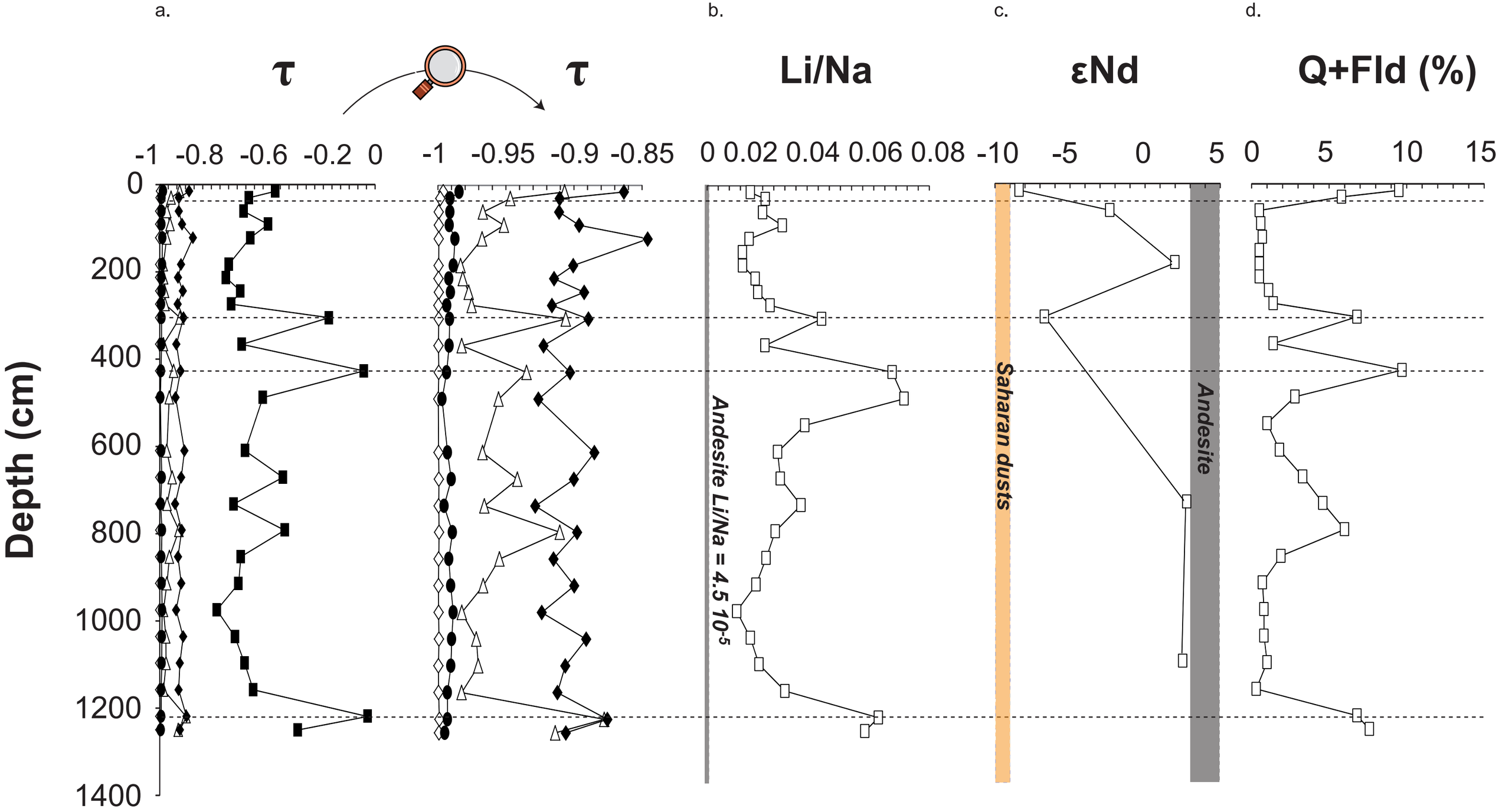
a.
b.
c.
d.
τ
τ
Li/Na
εNd
Q+Fld (%)
-1 -0.8 -0.6 -0.2 0
-1 -0.95 -0.9 -0.85
0 0.02 0.04 0.06 0.08
-10 -5 0 5
0 5 10 15
Depth (cm)
0
200
400
600
800
1000
1200
1400
Andesite Li/Na = 4.5 10-5
Saharan dusts
Andesite

Figure5

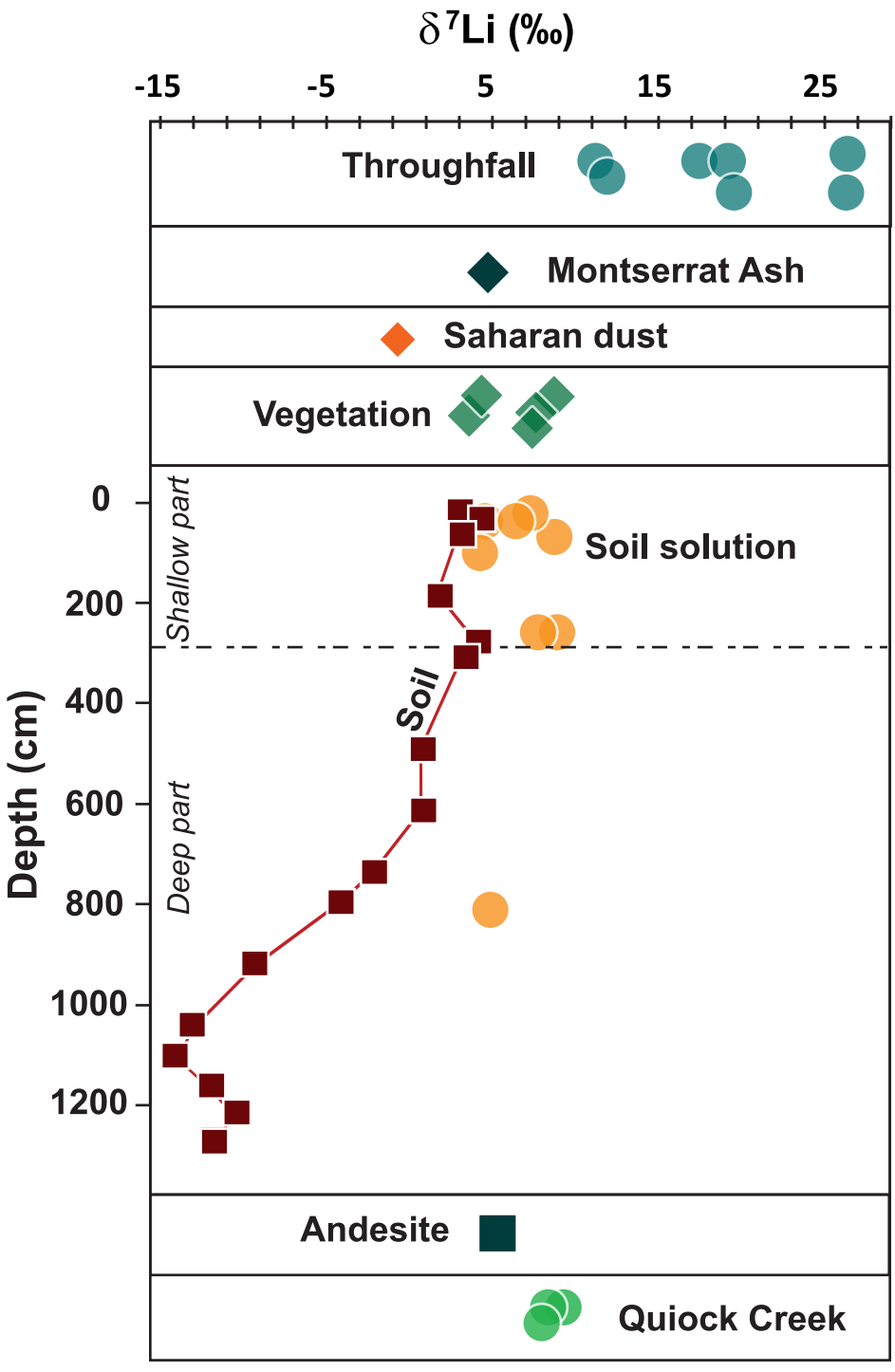
δ7Li (‰)
-15
-5
5
15
25
Throughfall
Montserrat Ash
Saharan dust
Vegetation
Soil solution
Shallow part
Soil
Deep part
Depth (cm)
0
200
400
600
800
1000
1200
Andesite
Quiock Creek

Figure6

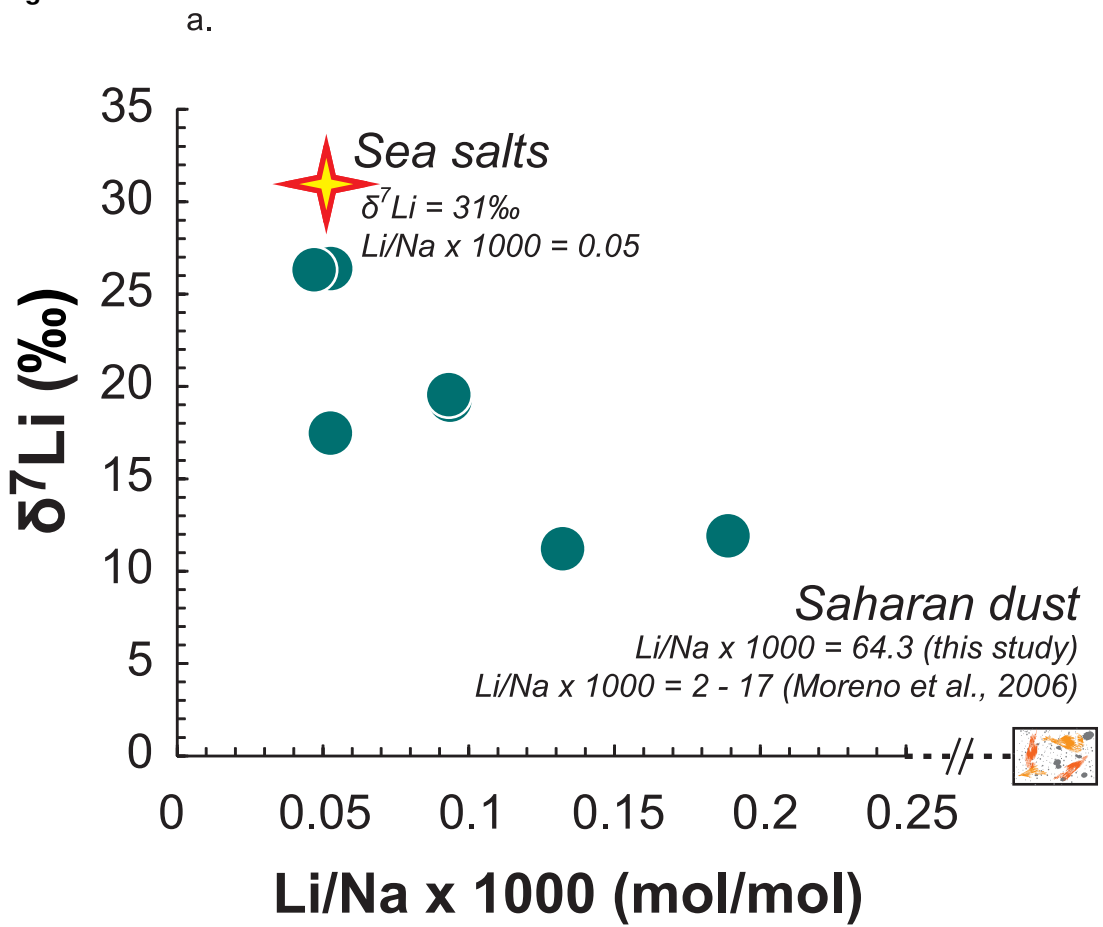
a.
Sea salts
δ7Li = 31‰
Li/Na x 1000 = 0.05
Saharan dust
Li/Na x 1000 = 64.3 (this study)
Li/Na x 1000 = 2 - 17 (Moreno et al., 2006)
δ7Li (‰)
Li/Na x 1000 (mol/mol)
0
5
10
15
20
25
30
35
0
0.05
0.1
0.15
0.2
0.25

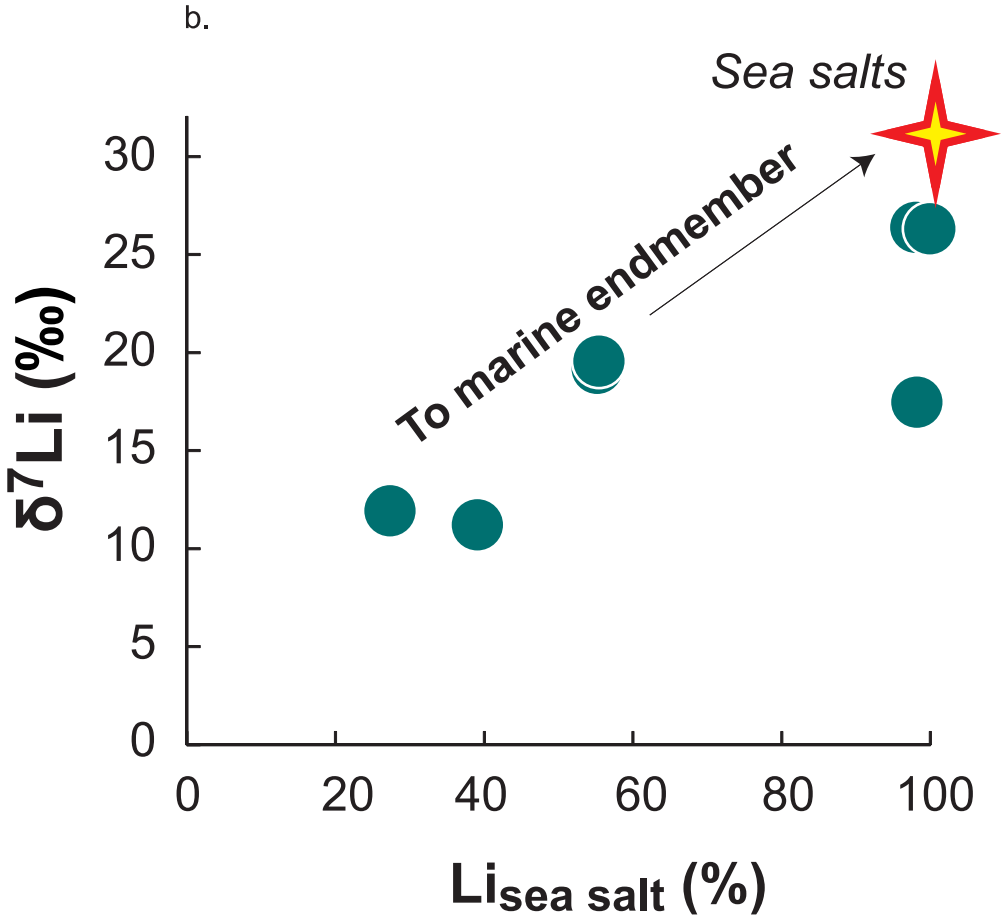
b.
Sea salts
To marine endmember
δ7Li (‰)
Lisea salt (%)
0
5
10
15
20
25
30
0
20
40
60
80
100

Figure7

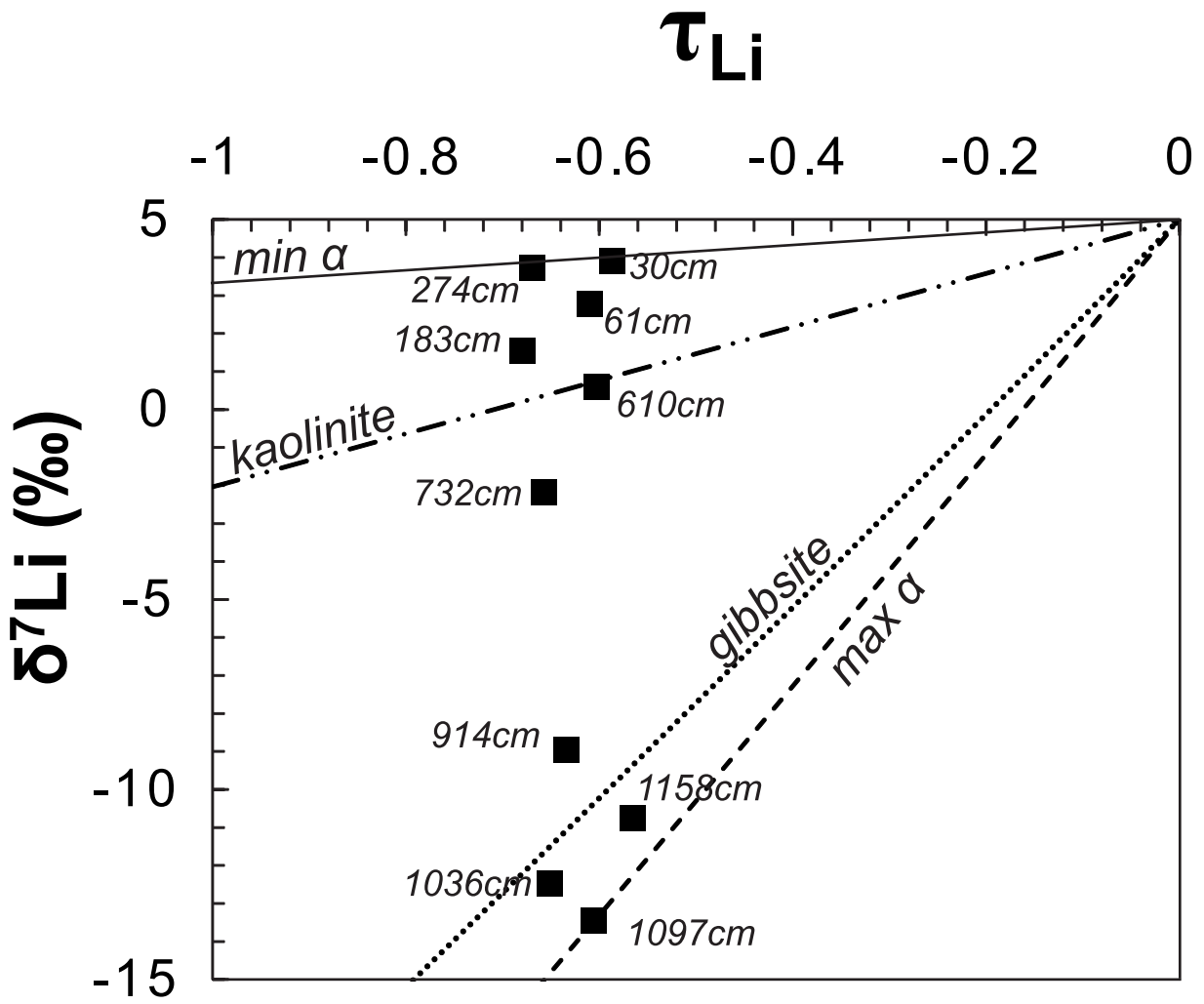
τLi
-1
-0.8
-0.6
-0.4
-0.2
0
5
0
-5
-10
-15
δ7Li (‰)
min α
274cm
30cm
61cm
183cm
610cm
kaolinite
732cm
gibbsite
max α
914cm
1158cm
1036cm
1097cm

Figure8

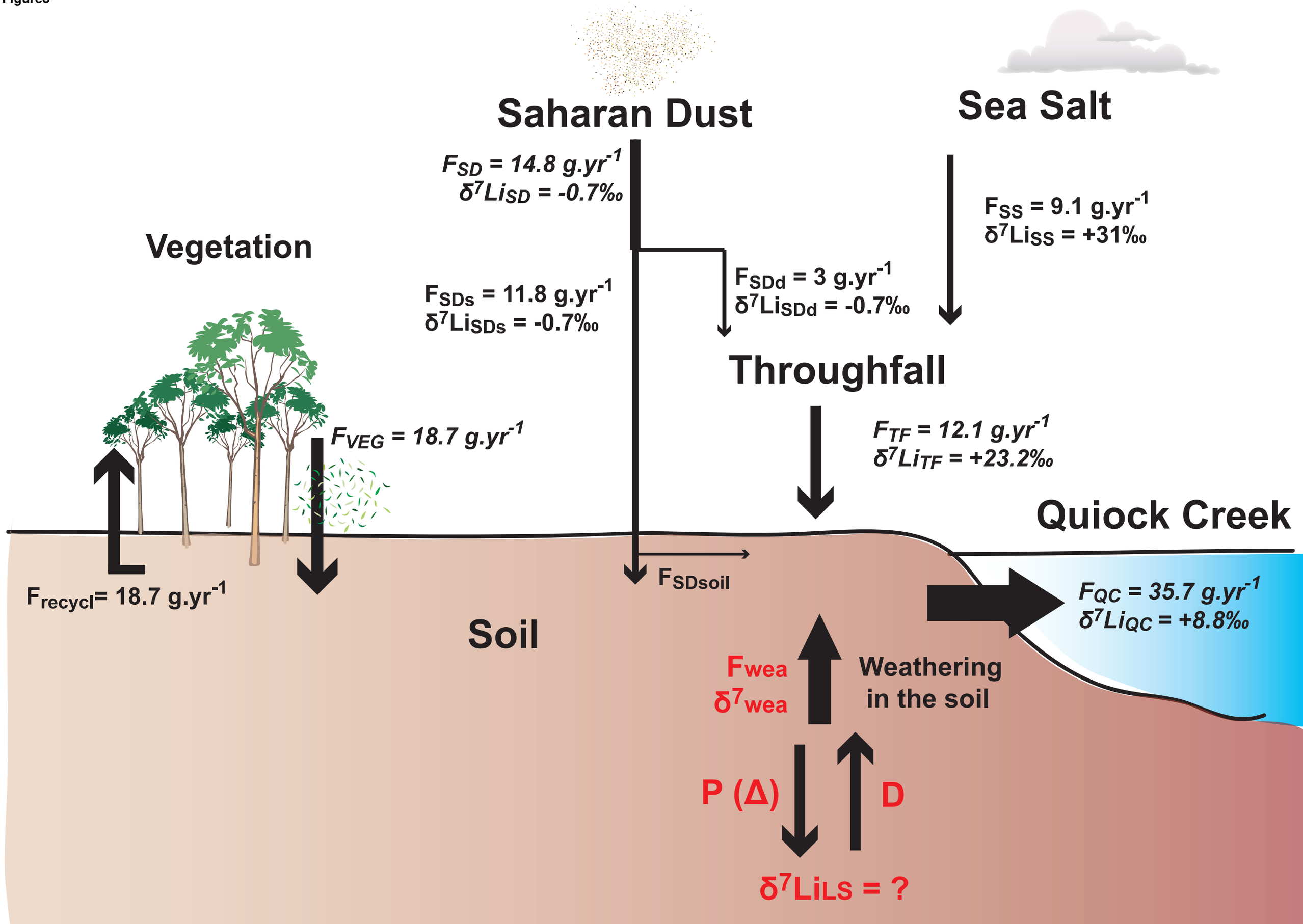
Saharan Dust
Sea Salt
F_{SD} = 14.8 g.yr^{-1}
δ^7Li_{SD} = -0.7‰
F_{SS} = 9.1 g.yr^{-1}
δ^7Li_{SS} = +31‰
Vegetation
F_{SDs} = 11.8 g.yr^{-1}
δ^7Li_{SDs} = -0.7‰
F_{SDd} = 3 g.yr^{-1}
δ^7Li_{SDd} = -0.7‰
Throughfall
F_{VEG} = 18.7 g.yr^{-1}
F_{TF} = 12.1 g.yr^{-1}
δ^7Li_{TF} = +23.2‰
Quiock Creek
F_{recycl}= 18.7 g.yr^{-1}
F_{SDsoil}
F_{QC} = 35.7 g.yr^{-1}
δ^7Li_{QC} = +8.8‰
Soil
F_{wea}
δ^7_{wea}
Weathering in the soil
P (Δ)
D
δ^7Li_{LS} = ?

Table

Click here to download Table: Table_Li.docx

Table 1: Cation, anion and Li concentrations and Li isotopic compositions of throughfall, stemflow, Quiock Creek and soil solution.

Sample name	Date	T	C	pH	Cl	Na	Si	K	HCO_3	Mg	SO_4	Ca	NO_3	Li	δ^7Li
		°C	µS		µmol/L	µmol/L	µmol/L	µmol/L	µmol/L	µmol/L	µmol/L	µmol/L	µmol/L	nmol/L	‰
Throughfalls															
TF collector n°1	10/08/2012			6.1	92	81	43	31	nd[1]	13	16	15.0	2	4	**17.5**
TF collector n°1	03/04/2013			nd	168	155	<[2]	26	nd	19	15	14.5	<	8	**26.4**
TF collector n°3	03/04/2013			nd	158	154	<	27	nd	18	15	14.1	<	7	**26.3**
TF collector n°1	25/06/2013			5.6	132	117	36	32	nd	17	16	16.9	<	11	**19.2**
Stemflow															
SF tree n°1	14/11/2011			nd	nd	316	nd	167	nd	106	17	143.6	<	29	**19.6**
SF tree n°2	18/11/2011			nd	nd	235	nd	131	nd	63	33	104.5	5	31	**11.2**
SF tree n°1	09/04/2012			3.6	nd	347	69	172	nd	103	24	149.0	<	66	**11.9**
Quiock Rill															
QC 1	23/04/2012	nd	nd	nd	229	184	109	6	37	25	15	10.5	<	42	**9.3**
QC 2	21/03/2013	22.6	43	4.8	274	211	112	3	28	32	13	14.9	<	45	**7.9**
QC 3	03/04/2013	22.6	39	4.6	249	217	112	5	34	28	15	12.1	<	38	**8.3**
QC 4	25/06/2013	24.2	38	nd	246	185	130	5	39	27	13	10.9	<	nd	**8.0**
Soil solution[3]															
GBD2 30	26/10/2012			4.8	169	166	nd	3.2	nd	26	15	1.4	5	57	**4.6**
GBD2 61	26/10/2012			4.8	164	147	nd	5.1	nd	31	19	10.7	26	53	**8.7**
GBD2 457	26/10/2012			4.5	168	194	nd	3.7	nd	14	13	1.9	<	68	**8.9**
GBD2 15	28/06/2013			nd	130	118	nd	1.6	nd	21	12	1.9	25	nd	**7.3**
GBD2 30	28/06/2013			5.4	150	147	nd	2.2	44	27	18	1.4	5	nd	**6.4**
GBD2 91	28/06/2013			5.3	207	194	nd	1.6	43	25	12	3.1	15	47	**4.3**
GBD2 457	28/06/2013			nd	165	153	nd	2.3	53	14	12	1.2	<	75	**7.7**
GBD2 823	28/06/2013			nd	242	204	nd	12.7	nd	14	15	0.6	<	79	**4.9**

[1] nd = not determined

[2] < = below detection (1.6 µmol L^{-1} for nitrates)

[3] For soil solution sample names GBD2 X, X = depth in cm.

Table 2: Major, Li and Ti concentrations and Li isotopic (‰) compositions of soil, andesite, dust and vegetation samples.

	Al	Fe	Mg	K	Na	Ca	Ti[1]	Li[2]	δ^7Li	εNd
	ppm	ppm	ppm	ppm	ppm	ppm	ppm	ppm	‰	
Soil										
GBD2_15	127354	96625	1977	1087	681	306	8573	11	2.7	-8.39
GBD2_30	103613	76592	1339	643	404	147	8873	8	3.9	
GBD2_61	155323	108098	1189	356	356	45	7913	7	2.8	-2.35
GBD2_91		90709	1207	455	295	43	6894	8		
GBD2_122		102804	1391	236	341	32	5336	5		
GBD2_152		102783	1564	292	452	51		6		
GBD2_183	153174	96955	1287	174	444	41	7674	6	1.5	1.92
GBD2_213		71214	1062	184	302	31	7374	5		
GBD2_244		85988	1326	226	347	51	7314	6		
GBD2_274	152976	79742	1043	249	248	28	7374	6	3.7	
GBD2_305	146994	106781	1499	1026	353	47	8033	15	3.0	-6.70
GBD2_366		92165	1068	194	344	35	8153	7		
GBD2_488	171413	116157	1262	615	158	28	10132	11	0.6	
GBD2_549	116900	80691	1041	164	209	26		7		
GBD2_610	162376	99738	1419	326	264	34	7314	7	0.6	
GBD2_671		58583	1041	491	309	42	6175	8		
GBD2_732	223894	80125	825	317	160	36	6834	5	-2.2	2.71
GBD2_792	161720	64526	880	621	278	43	5096	7	-4.1	
GBD2_853		80504	954	409	272	36	6654	6		
GBD2_914	162935	97945	1196	321	339	29	7074	6	-8.9	
GBD2_975	137066	93726	949	177	423	36	7374	5		
GBD2_1036		84111	1234	258	347	48	6714	5	-12.5	
GBD2_1097	159502	97153	946	242	291	23	5995	5	-13.5	2.44
GBD2_1158	146488	152338	1341	215	324	41	9052	9	-10.8	
GBD2_1219	135472	100878	1612	1276	277	78	7674	17	-8.8	
GBD2_1250	143788	100181	1312	971	215	60	8273	12	-10.5	
Andesite										
04GW12	95806	52600	9060	7308	27328	48462	5373	12	5.3	3-5[3]
Montserrat dust										
DMS 2010	84241	40537	15107	9406	26261	41158	3136	13	4.7	
Saharan dust										
SD 1	46151	23727	5355	5474	951	1747		20	-0.7	-10/-14[4]
SD 2	39693	20216	5059	5134	930	1918		17	-0.7	
Vegetation										
Root	464	252	1645	2839	2331	7284		345	4.3	

Branch	362	191	1728	4353	1921	11600	198	**3.6**
Litter 1	174	130	1930	2246	1828	10165	324	**8.7**
Litter 2	233	146	1960	2302	1857	10237	232	**7.6**
Litter 3	19606	328	5435	5106	2933	9993	413	**7.4**

[1] Ti concentrations in soil samples are from Buss et al. (2010).
[2] Li concentrations in vegetation given in ppb.
[3] Nd signature from White and Dupré (1986).
[4] Nd signature from Grousset et al. (1992).

Table 1S: ICP AES (for major elements) and ICP MS (for Li and Zr) analyses of rock and vegetation standard reference materials.

	Al	Ca	Fe	K	Mg	Na	Li
	ppm	ppm	ppm	ppm	ppm	ppm	ppm
Rock standards							
BEN certif[1]	53312	99071	8988	11534	789	23594	13
BEN (this study)	54289	99897	90935	11739	79269	23846	15
	5214	95138	89888	11397	76588	23325	
GSN certif[1]	77665	17857	2625	38419	138	27971	55
GSN (this study)	77987	17562	25798	35813	13629	26838	54.6
	77673	17467	25594	35454	136	26723	56.1
	80519	17834	26123	37214	1377	27587	50.9
BCR-2 certif[2]	71471	50857	966	14853	2154	23445	9
BCR-2 (this study)	72353	50762	93866	13885	21555	22619	9.96
BHVO-2 certif[2]	71471	81429	8638	4315	4338	16471	5
BHVO-2 (this study)	7056	7895	8321	3957	42096	15813	5.1
	73674	82099	87389	4184	44552	16492	4.4
JB-2 certif [3]	77267	70683	100299	3487	28103	1506	8
JB-2 (this study)	77245	70136	95777	3058	2739	14046	8.9
							7.9
Vegetation standard							
NIST_SRM 1515 (certif)	286	15260	83	16000	2700	24	
NIST_SRM 1515 (this study)	283	14441	69	15216	2421	55	305[4]
	290	14349	73	15544	2478	57	
	283	14872	75	16102	2662	42	
	286	15014	76	16307	2682	42	

[1] Recommended values of GSN, BEN are taken from CRPG certificate of analyse (http://helium.crpg.cnrs-nancy.fr/SARM/pages/geostandards.html#).
[2] Recommended values of BHVO-2 and BCR-2 are taken from USGS certificate of analyses (http://crustal.usgs.gov/geochemical_reference_standards/).
[3] JB2 is a GSJ (Geological Survey of Japan) reference rock standards (http://georem.mpch-mainz.gwdg.de/sample_query.asp).
4 Vegetation Li concentration in ppb

Table 3S: Cation, anion and Li concentrations of throughfall, stemflow, Quiock Creek (QC) and soil solution (GBD2_L) samples.

Sample name	Date	T	C	pH	Na	Cl	Si	K	Ca	Mg	Alc	SO_4	NO_3	Li
		°C			µmol/L	µmol/L	µmol/L	µmol/L	µmol/L	µmol/L	µmol/L	µmol/L	µmol/L	nmol/L
Throughfall														
TF collector n°1	14/11/2011	nd[1]	nd	nd	213	nd	nd	108	28	32	nd	nd	nd	20
TF collector n°2	14/11/2011	nd	nd	nd	177	nd	nd	50	30	29	nd	nd	nd	16
TF collector n°1	21/11/2011	nd	nd	5.49	21	23	nd	11	5	4	nd	7.5	4.6	3
TF collector n°3	21/11/2011	nd	nd	5.8	71	78	nd	34	8	8	nd	13.0	8.0	5
TF collector n°1	25/11/2011	nd	nd	nd	36	nd	nd	26	8	7	nd	nd	nd	6
TF collector n°2	25/11/2011	nd	nd	nd	26	nd	nd	22	8	5	nd	nd	nd	3
TF collector n°3	25/11/2011	nd	nd	nd	57	nd	nd	35	8	6	nd	nd	nd	4
TF collector n°1	09/04/2012	nd	nd	nd	124	nd	36	61	23	23	nd	nd	nd	3
TF collector n°2	09/04/2012	nd	nd	nd	124	nd	31	62	26	23	nd	nd	nd	13
TF collector n°3	09/04/2012	nd	nd	nd	125	nd	nd	42	16	17	nd	nd	nd	11
TF collector n°1	13/04/2012	nd	nd	nd		nd	42	94	35	40	nd	nd	nd	20
TF collector n°2	13/04/2012	nd	nd	nd		nd	39	68	34	31	nd	nd	nd	16
TF collector n°3	13/04/2012	nd	nd	nd	180	204	47	68	33	29	nd	21.9	<	16
TF collector n°2	16/04/2012	nd	nd	nd	100	119	15	30	14	13	nd	13	<	9
TF collector n°3	16/04/2012	nd	nd	nd		107	15				nd	13	<	7
TF collector n°1	19/04/2012	nd	nd	nd	199	nd	32	57	29	29	nd	nd	nd	13
TF collector n°2	19/04/2012	nd	nd	nd	215	nd	27	52	30	35	nd	nd	nd	13
TF collector n°3	19/04/2012	nd	nd	nd	254	nd	38	47	25	35	nd	nd	nd	13
TF collector n°1	23/04/2012	nd	nd	nd	17	nd	8	17	5	4	nd	nd	nd	3
TF collector n°2	23/04/2012	nd	nd	nd	19	nd	36	14	5	4	nd	nd	nd	3
TF collector n°3	23/04/2012	nd	nd	nd	25	nd	7	10	3	3	nd	nd	nd	3
TF collector n°1	05/08/2012	nd	nd	6.02	83	93	35	33	8	10	nd	12.3	<	5
TF collector n°2	05/08/2012	nd	nd	5.96	72	84	34	21	10	9	nd	9.5	<	<
TF collector n°3	05/08/2012	nd	nd	6.18	89	89	49	22	11	9	nd	11.5	<	<
TF collector n°1	10/08/2012	nd	nd	6.08	81	92	43	31	15	13	nd	15.5	1.6	4
TF collector n°2	10/08/2012	nd	nd	6.33	74	88	47	30	18	14	nd	13.7	1.2	4
TF collector n°3	10/08/2012	nd	nd	5.65	104	94	73	31	31	17	nd	16.6	5.1	4
TF collector n°1	16/08/2012	nd	nd	6.05	196	224	44	41	25	25	nd	28.3	4.4	13
TF collector n°2	16/08/2012	nd	nd	6.29	238	259	67	56	30	28	nd	28.1	<	18
TF collector n°3	16/08/2012	nd	nd	6.19	264	264	81	57	36	32	nd	29.4	6.7	17
TF collector n°1	21/03/2013	nd	nd	5.74	71	67	<[2]	16	5	7	nd	7.6	<	4
TF collector n°3	21/03/2013	nd	nd	5.6	71	64	<	13	6	7	nd	8.1	<	<
TF collector n°1	25/03/2013	nd	nd	nd	nd	nd	34	nd	nd	nd	nd	nd	nd	13
TF collector n°3	25/03/2013	nd	nd	5.76	152	150	48	62	19	20	nd	18.6	<	9
TF collector n°1	27/03/2013	nd	nd	5.09	177	211	44	78	24	28	nd	17.2	<	<
TF collector n°3	27/03/2013	nd	nd	nd	193	182	66	52	21	23	nd	20.3	<	<
TF collector n°1	29/03/2013	nd	nd	5.73	167	190	31	70	25	27	nd	25.0	<	<
TF collector n°3	29/03/2013	nd	nd	5.75	196	178	55	52	20	23	nd	28.0	<	<
TF collector n°1	01/04/2013	nd	nd	5.5	43	44	<	16	6	6	nd	6.8	<	2
TF collector n°3	01/04/2013	nd	nd	5.49	48	42	<	18	6	6	nd	7.7	<	2
TF collector n°1	03/04/2013	nd	nd	nd	155	168	<	26	14	19	nd	15.1	<	8

TF collector n°3	03/04/2013	nd	nd	nd	154	158	<	27	14	18	nd	15.1	<	7
TF collector n°1	25/06/2013	nd	nd	5.58	117	132	36	32	17	17	nd	15.5	<	11
TF collector n°3	25/06/2013	nd	nd	5.63	164	177	<	43	21	26	nd	21.5	<	13
TF collector n°1	26/06/2013	nd	nd	5.94	83	99	<	23	11	12	nd	9.9	<	6
TF collector n°3	26/06/2013	nd	nd	5.83	91	99	750	21	12	11	nd	10.3	<	4
TF collector n°1	28/06/2013	nd	nd	5.74	66	74	<	16	11	11	nd	9.5	<	5
Stemflow														
SF tree n°1	14/11/2011	nd	nd	nd	316	pol	nd	167	144	106	nd	17.5	<	29
SF tree n°2	18/11/2011	nd	nd	nd	235	pol	nd	131	104	63	nd	33.5	4.6	31
SF tree n°1	09/04/2012	nd	nd	3.55	347	pol	69	172	149	103	nd	23.8	<	66
Rainfall														
RF-MF 1	09/04/2012	nd	22.59	5.3	69	86	nd	3	8	8	nd	10	<	<
RF-MF 2	13/04/2012	nd	nd	nd	137	167	nd	5	10	17	nd	15	<	<
RF-MF 3	16/04/2012	nd	nd	4.93	87	110	nd	3	4	11	nd	11	<	<
RF-MF 4	19/04/2012	nd	nd	nd	165	nd	nd	6	11	22	nd		nd	9
RF-MF 5	23/04/2012	nd	nd	nd	69	73	nd	1	1	1	nd	8	<	<
RF-MF 6	03/08/2012	nd	nd	4.93	65	55	nd	3	15	10	nd	4	<	6
RF-MF 7	10/08/2012	nd	nd	5.65	48	54	nd	1	15	10	nd	6	<	<
RF-OVSG 1	20/03/2013	nd	nd	4.77	82	85	nd	3	2	10	nd	7.4	<	4
RF-OVSG 2	21/03/2013	nd	nd	4.51	71	75	nd	4	4	10	nd	8.0	<	<
RF-OVSG 3	27/03/2013	nd	nd	nd	127	133	nd	5	7	16	nd	12.1	<	<
RF-OVSG 4	31/03/2013	nd	nd	4.69	41	49	nd	2	3	5	nd	5.8	4.2	<
RF-OVSG 5	01/04/2013	nd	nd	4.09	121	131	nd	4	4	15	nd	10.9	3.0	<
RF-OVSG 6	04/04/2013	nd	nd	5.14	76	88	nd	9	7	13	nd	7.4	<	4
Quiock Creek														
QC	21/06/2011	25	nd	5.67	261	nd	nd	5	10	29	27.2	nd	<	nd
QC	08/07/2011	24.1	34.3	5.51	2016	nd	nd	7	13	24	25.2	nd	<	nd
QC	19/08/2011	24.1	38	5.3	213	nd	nd	6	12	25	28.4	nd	<	nd
QC	16/09/2011	24.1	nd	4.65	247	nd	nd	4	9	28	26.9	nd	<	nd
QC	14/10/2011	23.8	29	5.5	241	nd	nd	4	10	28	28.4	nd	<	68
QC	08/11/2011	23.9	22.49	4.85	226	nd	nd	5	10	26	67.5	nd	<	nd
QC	08/11/2011	24	33.3	4.98	227	nd	nd	5	10	26	73.8	nd	1.8	nd
QC	09/11/2011	24.1	31	5.45	234	nd	nd	5	10	27	43.1	nd	1.5	nd
QC	09/11/2011	nd	nd	nd	237	nd	nd	4	10	27	nd	nd	1.6	nd
QC	10/11/2011	23.5	31.5	5.48	212	nd	nd	5	10	25	49.3	nd	1.8	41
QC	10/11/2011	23.8	31.4	5.55	222	nd	nd	5	10	26	88.2	nd	1.6	nd
QC	11/11/2011	23.8	33.8	5.3	235	nd	nd	4	10	28	48.9	nd	1.6	nd
QC	12/11/2011	23.4	36.5	5.38	239	nd	nd	4	9	28	44.4	nd	1.8	nd
QC	14/11/2011	23.3	31.7	5.38	244	nd	nd	4	9	28	44.8	nd	1.5	nd
QC	15/11/2011	23.3	34.1	5.13	246	nd	nd	4	9	29	33.4	nd	1.6	nd
QC	16/11/2011	23	53.6	5.3	244	nd	nd	4	9	29	26.2	nd	1.9	nd
QC	18/11/2011	23.3	33.3	5.38	249	nd	nd	7	11	29	13.8	nd	1.5	nd
QC	21/11/2011	21.8	32.4	5.35	207	nd	nd	4	9	30	12.5	nd	1.9	nd
QC	23/11/2011	23.2	33.4	5.56	247	nd	nd	4	8	29	23.4	nd	1.6	48
QC	09/12/2011	23	68.2	5.56	218	nd	nd	4	9	27	nd	nd	<	59
QC	06/01/2012	22.5	32.5	4.95	233	nd	135	5	9	29	26.6	nd	1.6	63

QC	03/02/2012	21.6	38	5.15	239	nd	152	5	8	30	nd	nd	1.8	72
QC	16/03/2012	21.6	49.8	4.75	254	nd	148	7	10	31	7.2	nd	<	72
QC	04/04/2012	22.8	nd	nd	245	298	162	6	9	28	40.5	12.1	<	62
QC	09/04/2012	22.3	48.1	5.2	218	282	149	8	10	29	34.1	14.0	<	60
QC	13/04/2012	23	45.9	5.31	258	298	142	9	10	30	nd	13.0	<	62
QC	19/04/2012	22.5	42.7	5.49	199	nd	nd	7	14	31	29.7	nd	6.1	47
QC	23/04/2012	nd	nd	nd	184	229	109	6	11	25	37.0	15.5	<	42
QC	26/04/2012	23.7	42.5	5.22	220	nd	nd	6	10	26	38.0	nd	3.4	55
QC	08/06/2012	23.8	51	5.54	262	nd	nd	4	8	30	37.0	nd	1.8	61
QC	03/08/2012	24.3	45	nd	248	271	303	5	9	29	41.6	13.5	<	54
QC	05/08/2012	24.9	25.8	5.12	234	257	278	5	10	27	nd	13.2	<	50
QC	10/08/2012	24.2	46.1	5.9	237	253	268	5	9	28	30.7	13.3	<	54
QC	16/08/2012	24.3	47.4	5.2	253	275	300	5	8	29	34.4	13.1	<	60
QC	07/09/2012	23.7	30.9	4.34	264	nd	nd	3	7	30	31.1	nd	1.6	65
QC	05/10/2012	23.8	38.6	4.63	243	nd	nd	4	8	28	9.2	nd	1.6	56
QC	23/10/2012	23.6	40.3	4.9	250	269	300	5	10	29	36.4	12.4	<	59
QC	26/10/2012	24	40	4.65	254	271	304	4	8	30	23.3	11.8	<	60
QC	30/11/2012	23.4	41.8	5.03	263	nd	nd	12	9	30	8.0	nd	<	63
QC	14/12/2012	22.3	44.7	4.92	264	nd	nd	6	9	31	43.3	nd	<	60
QC	18/01/2013	nd	nd	5.06	269	nd	nd	6	9	32	33.6	nd	<	62
QC	01/02/2013	21.9	30.6	5.23	264	nd	152	8	10	32	28.4	nd	<	58
QC	01/03/2013	21.1	51.3	5.45	258	nd	177	5	10	32	9.2	nd	<	71
QC	20/03/2013	22.1	49	5.22	282	315	151	10	13	35	24.4	13.8	<	59
QC	21/03/2013	22.6	43	4.78	211	274	112	3	15	32	27.5	12.9	<	45
QC	25/03/2013	23.3	44	4.92	258	283	167	7	11	30	13.4	12.9	<	57
QC	26/03/2013	nd	nd	nd	208	nd	nd	4	11	29	nd	nd	<	nd
QC	27/03/2013	nd	nd	5.26	251	276	161	7	11	30	24.8	12.1	<	nd
QC	29/03/2013	23	43	5.32	250	279	153	8	11	30	23.9	14.5	<	49
QC	01/04/2013	22.2	40	4.57	224	263	129	5	12	28	17.2	12.9	<	40
QC	03/04/2013	22.6	39	4.6	217	249	112	5	12	28	33.6	14.7	<	38
QC	24/05/2013	23.4	38.8	5.29	203	265	145	3	9	28	31.1	11.9	<	nd
QC	21/06/2013	23.9	43	nd	209	288	148	3	10	30	40.0	11.3	<	59
QC	25/06/2013	24.2	38	nd	185	246	130	5	11	27	39.2	12.7	<	nd
QC	26/06/2013	23.9	39.4	5.1	189	260	133	3	11	28	65.6	12.1	<	47
QC	28/06/2013	24	40.5	5.17	200	275	144	3	9	30	29.7	11.7	<	52
QC	02/07/2013	23.6	40.3	5.27	202	277	147	3	10	30	11.1	11.6	<	51
Soil solution[3]														
GBD2 15 L	08/07/2011	nd	nd	4.82	117	103	nd	3.8	2.85	21	nd	20.3	27.4	52
GBD2 61 L	08/07/2011	nd	nd	4.79	131	135	nd	3.5	8.63	28	nd	31.0	6.8	41
GBD2 91 L	08/07/2011	nd	nd	4.93	245	241	nd	4.3	4.46	28	nd	14.3	31.9	98
GBD2 457 L	08/07/2011	nd	nd	4.83	204	205	nd	3.7	0.25	11	nd	11.4	<	95
GBD2 823 L	08/07/2011	nd	nd	4.68	252	259	nd	14.0	0.88	13	nd	16.8	<	78
GBD2 30 L	16/03/2012	nd	nd	5.2	170	143	nd	14.1	4.68	29	nd	18.8	5.3	nd
GBD2 61 L	16/03/2012	nd	nd	4.64	125	149	nd	5.9	13.63	32	nd	26.6	16.6	nd
GBD2 91 L	16/03/2012	nd	nd	4.99	237	229	nd	3.6	3.09	22	nd	15.0	20.3	121
GBD2 457 L	16/03/2012	nd	nd	5.28	266	197	nd	38.8	6.65	16	nd	19.1	<	112

GBD2 823 L	16/03/2012	nd	nd	4.88	243	256	nd	13.8	1.93	17	nd	18.0	<	105
GBD2 91 L	26/04/2012	nd	nd	5.16	216	230	nd	3.5	4.01	26	nd	12.7	17.3	59
GBD2 457 L	26/04/2012	nd	nd	4.88	188	182	nd	6.0	3.62	15	nd	16.5	<	101
GBD2 823 L	26/04/2012	nd	nd	4.61	211	252	nd	14.1	1.94	17	nd	15.3	<	116
GBD2 15 L	08/06/2012	nd	nd	4.96	112	124	nd	4.2	3.29	25	nd	14.1	19.8	56
GBD2 91 L	08/06/2012	nd	nd	5.02	228	232	nd	3.2	3.88	26	nd	12.6	17.4	70
GBD2 457 L	08/06/2012	nd	nd	5.09	184	182	nd	4.8	2.93	14	nd	15.8	<	95
GBD2 823 L	08/06/2012	nd	nd	4.78	211	247	nd	13.9	4.42	15	nd	15.0	<	108
GBD2 15 L	05/10/2012	nd	nd	4.82	129	101	nd	4.1	2.50	23	nd	10.5	72.9	62
GBD2 30 L	05/10/2012	nd	nd	4.49	182	213	nd	5.4	2.24	28	nd	13.3	7.6	79
GBD2 91 L	05/10/2012	nd	nd	4.49	243	237	nd	4.3	3.36	23	nd	11.0	26.5	89
GBD2 457 L	05/10/2012	nd	nd	4.4	195	176	nd	4.9	1.99	14	nd	14.3	<	nd
GBD2 823 L	05/10/2012	nd	nd	5	244	257	nd	16.7	0.40	14	nd	16.1	<	97
GBD2 15 L	26/10/2012	nd	nd	4.57	112	85	nd	1.8	1.49	17	nd	13.0	33.1	48
GBD2 30 L	26/10/2012	nd	nd	4.75	166	169	nd	3.2	1.45	26	nd	14.8	5.0	57
GBD2 61 L	26/10/2012	nd	nd	4.49	147	164	nd	5.1	10.72	31	nd	19.5	25.8	53
GBD2 91 L	26/10/2012	nd	nd	5.14	226	211	nd	2.8	2.74	21	nd	11.0	17.4	63
GBD2 457 L	26/10/2012	nd	nd	4.46	194	168	nd	3.7	1.86	14	nd	13.2	<	68
GBD2 91 L	21/06/2013	nd	nd	nd	173	182	nd	1.9	2.53	21	57.5	11.6	<	49
GBD2 457 L	21/06/2013	nd	nd	nd	153	165	nd	2.3	1.20	14	52.8	11.7	<	75
GBD2 823 L	21/06/2013	nd	nd	nd	204	242	nd	12.7	0.65	14	nd	15.3	<	79
GBD2 15 L	28/06/2013	nd	nd	nd	118	130	nd	1.6	1.85	21	nd	12.4	25.0	nd
GBD2 30 L	28/06/2013	nd	nd	5.35	147	150	nd	2.2	1.36	27	43.9	17.5	5.5	nd
GBD2 91 L	28/06/2013	nd	nd	5.28	194	207	nd	1.6	3.13	25	43.3	11.8	15.3	47
GBD2 457 L	28/06/2013	nd	nd	5.41	159	167	nd	2.9	1.52	14	38.0	12.1	2.6	71
GBD2 823 L	28/06/2013	nd	nd	nd	210	243	nd	13.4	0.97	15	29.7	15.6	<	76

[1] nd = not determined

[2] < = below detection (1.6 µmol L^{-1} for nitrates)

[3] For soil solution sample names GBD2 X, X = depth in cm.